Inorg. Chem. **2008**, *47*, 9021−9034

High-Yield Syntheses and Reactivity Studies of Fe_{10} "Ferric Wheels": Structural, Magnetic, and Computational Characterization of a Star-Shaped Fe_8 Complex

Theocharis C. Stamatatos,[†] Alexander G. Christou,[†] Shreya Mukherjee,[†] Katye M. Poole,[‡] Christos Lampropoulos,[†] Khalil A. Abboud,[†] Ted A. O'Brien,[‡,§] and George Christou*[,†]

Department of Chemistry, University of Florida, Gainesville, Florida 32611-7200, and Department of Chemistry and Chemical Biology, Indiana University-Purdue University Indianapolis, Indianapolis, Indiana 46202-3274

Received June 5, 2008

Convenient, high-yield routes have been developed to $[Fe_{10}(OMe)_{20}(O_2CR)_{10}]$ (**1**) "ferric wheels" involving the alcoholysis of $[Fe_3O(O_2CR)_6(H_2O)_3]^+$ salts in MeOH in the presence of NEt_3. Reactivity studies have established $[Fe_{10}(OMe)_{20}(O_2CMe)_{10}]$ (**1a**) to undergo clean carboxylate substitution with a variety of other RCO_2H groups to the corresponding $[Fe_{10}(OMe)_{20}(O_2CR)_{10}]$ product. In contrast, the reaction with phenol causes a nuclearity change to give a smaller $[Fe_8(OH)_4(OPh)_8(O_2CR)_{12}]$ (**2**) wheel. Similarly, reactions of $[Fe_{10}(OMe)_{20}(O_2CR)_{10}]$ with the bidentate chelate ethylenediamine (en) cause a structural change to give either $[Fe_8O_5(O_2CMe)_8(en)_8](ClO_4)_6$ (**3**) or $[Fe_2O(O_2CBu^t)(en)_4](NO_3)_3$ (**4**), depending on conditions. Complex **3** possesses a "Christmas-star" Fe_8 topology comprising a central planar $[Fe_4(\mu_4\text{-}O)]^{10+}$ square subunit edge-fused to four oxide-centered $[Fe_3(\mu_3\text{-}O)]^{7+}$ triangular units. Variable-temperature, solid-state dc and ac magnetization studies on complexes **1a**−**4** in the 5.0−300 K range established that all the complexes possess an $S = 0$ ground state. The magnetic susceptibility data for **4** were fit to the theoretical χ_M versus T expression derived by the use of an isotropic Heisenberg spin Hamiltonian and the Van Vleck equation, and this revealed an antiferromagnetic exchange parameter with a value of $J = -107.7(5)$ cm^{-1}. This value is consistent with that predicted by a previously published magnetostructural relationship. Theoretically computed values of the exchange constants in **3** were obtained with the ZILSH method, and the pattern of spin frustration within its core and the origin of its $S = 0$ ground state have been analyzed in detail.

Introduction

Polynuclear clusters of Fe continue to be the objects of synthesis and study by many groups around the world. This is a reflection of the diverse areas to which such chemistry is relevant, from magnetic materials to mineralogy and biology. Molecular oxide-bridged iron(III) clusters with structural or other relevance to minerals such as hematite or ferrihydrite,[1] the iron-oxo-hydroxo core of the iron storage protein ferritin,[2] and biomineralization in general[3] are some of the areas of interest in high-nuclearity Fe chemistry. Smaller nuclearity molecules are also of biological interest, such as those containing the $[Fe_2(\mu\text{-}O)(O_2CR)_2]^{2+}$ core of the oxygen carrier protein hemerythrin[4] and the related cores in other dinuclear Fe proteins such as ribonucleotide reductases,[5] purple acid phosphatases,[6] and methane monooxygenases.[7]

* To whom correspondence should be addressed. E-mail: christou@chem.ufl.edu.
[†] University of Florida.
[‡] Indiana University-Purdue University Indianapolis.
[§] Deceased.

(1) Ammala, P. S.; Batten, S. R.; Cashion, J. D.; Kepert, C. M.; Moubaraki, B.; Murray, K. S.; Spiccia, L.; West, B. O. *Inorg. Chim. Acta* **2002**, *331*, 90.

(2) (a) Theil, E. C. *Annu. Rev. Biochem.* **1987**, *57*, 289. (b) Xu, B.; Chasteen, N. D. J. *Biol. Chem.* **1991**, *266*, 19965. (c) Bertini, I.; Gray, H. B.; Lippard, S. J.; Valentine, J. S. *Bioinorganic Chemistry*; University Science Books: Mill Valley, CA, 1994. (d) Theil, E. C.; Matzapetakis, M.; Liu, X. *J. Biol. Inorg. Chem.* **2006**, *11*, 803. (e) Grant, R. A.; Filman, D. J.; Finkel, S. E.; Kolter, R.; Hogle, J. M. *Nat. Struct. Biol.* **1998**, *5*, 294.

(3) (a) Taft, K. L.; Papaefthymiou, G. S.; Lippard, S. J. *Science* **1993**, *259*, 1302. (b) Gorun, S. M.; Papaefthymiou, G. S.; Frankel, R. B.; Lippard, S. J. *J. Am. Chem. Soc.* **1987**, *109*, 4244. (c) Powell, A. K. *Struct. Bonding (Berlin)* **1997**, *88*, 1; and references therein.

10.1021/ic801038r CCC: $40.75
Published on Web 08/13/2008

Another important aspect of polynuclear iron complexes is their often interesting magnetic properties. Although oxo-bridged Fe^{III} atoms are almost always antiferromagnetically coupled, some Fe_x clusters exhibit spin frustration effects or display particular topologies that result in a reasonably large ground-state spin (S).[8] In some cases, this is accompanied by a significant magnetoanisotropy, leading to single-molecule magnets.[9] The latter are molecules that display slow magnetization relaxation rates and which, below their blocking temperature (T_B), function as single-domain magnetic particles of nanoscale dimensions.[10] Examples include certain Fe_4,[11] Fe_8,[12] Fe_9,[13] and Fe_{19},[14] among others.[10b] Such single-molecule magnets thus represent a molecular, "bottom-up" approach to nanomagnetism.[10a]

Single-strand wheels and closed, cage-like clusters are the two families of polynuclear iron complexes that have attracted the most interest in recent years, and both families include complexes of high nuclearity and aesthetically pleasing architecture. Of relevance to the present work are single-strand Fe^{III} wheels, which almost always contain an even number of metal atoms and are antiferromagnetically coupled with $S = 0$ ground states.[15] Such molecules represent a very rare amalgamation of high nuclearity and high magnetic symmetry, the latter referring to the (often) single type of Fe_2 pairwise exchange couplings they contain. Thus, they represent excellent model systems for the study of one-dimensional magnetism (especially if a family of related wheels with differing numbers of metal atoms can be obtained), magnetic anisotropy,[16] and quantum effects such as coherent tunneling of the Néel vector.[17] The prototype single-strand wheel was $[Fe(OMe)_2(O_2CCH_2Cl)]_{10}$, dubbed the "ferric wheel ",[18] which was also later reported with other carboxylates.[15a,19] Many other Fe_x wheels have since been reported and now comprise the largest family of known molecular wheels.[20−22]

Studies on Fe_{10} ferric wheels have typically been limited to basic characterization of isolated materials by crystallography and magnetic studies, and a major reason for this has been that in almost every case the compounds were obtained by accident, usually in low yields (up to 40%, but typically much less), and/or from precursors that were themselves not readily accessible.[15a,18−20] This has hampered easy access to derivatives for comparative study or their use as starting materials for reactivity studies aimed at accessing new products. Therefore, as part of our recently initiated program directed toward developing new synthetic routes

(4) (a) Kurtz, D. M., Jr. *Chem. Rev.* **1990**, *90*, 585. (b) Lippard, S. J. *Angew. Chem., Int. Ed. Engl.* **1988**, *27*, 344. (c) Toftlund, H.; Murray, K. S.; Zwack, P. R.; Taylor, L. F.; Anderson, O. P. *J. Chem. Soc., Chem. Commun.* **1986**, 191. (d) Wilkins, P. C.; Wilkins, R. G. *Coord. Chem. Rev.* **1987**, *79*, 195. (e) Vincent, J. B.; Huffman, J. C.; Christou, G.; Li, Q.; Nanny, M. A.; Hendrickson, D. N.; Fong, R. H.; Fish, R. H. *J. Am. Chem. Soc.* **1988**, *110*, 6898.

(5) (a) Bunker, G.; Petersson, L.; Sjoberg, B.- M.; Sahlin, M.; Chance, M.; Chance, B.; Ehrenberg, A. *Biochemistry* **1987**, *26*, 4708. (b) Scarrow, R. C.; Maroney, M. J.; Palmer, S. M.; Que, L.; Roe, A. L.; Salowe, S. P.; Stubbe, J. *J. Am. Chem. Soc.* **1987**, *109*, 7857. (c) Sjoberg, B. M.; Sanders-Loehr, J.; Loehr, T. M. *Biochemistry* **1987**, *26*, 4242.

(6) Averill, B. A.; Davis, J. C.; Burman, S.; Zirino, T.; Sanders-Loehr, J.; Loehr, T. M.; Sage, J. T.; Debrunner, P. G. *J. Am. Chem. Soc.* **1987**, *109*, 3760; and references therein.

(7) (a) Prince, R. C.; George, G. N.; Savas, J. C.; Cramer, S. P.; Patel, R. N. *Biochim. Biophys. Acta* **1988**, *952*, 220. (b) Ericson, A.; Hedman, B.; Hodgson, K. O.; Green, J.; Dalton, H.; Bentsen, J. G.; Beer, R. H.; Lippard, S. J. *J. Am. Chem. Soc.* **1988**, *110*, 2330. (c) Dalton, H. *Adv. Appl. Microbiol.* **1980**, *26*, 71. (d) Woodland, M. P.; Dalton, H. *J. Biol. Chem.* **1984**, *259*, 53.

(8) (a) Jones, L. F.; Brechin, E. K.; Collison, D.; Helliwell, M.; Mallah, T.; Piligkos, S.; Rajaraman, G.; Wernsdorfer, W. *Inorg. Chem.* **2003**, *42*, 6601. (b) Powell, A. K.; Heath, S. L.; Gatteschi, D.; Pardi, L.; Sessoli, R.; Spina, G.; Del Giallo, F.; Pieralli, F. *J. Am. Chem. Soc.* **1995**, *117*, 2491. (c) McCusker, J. K.; Vincent, J. B.; Schmitt, E. A.; Mino, M. L.; Shin, K.; Coggin, D. K.; Hagen, P. M.; Huffman, J. C.; Christou, G.; Hendrickson, D. N. *J. Am. Chem. Soc.* **1991**, *113*, 3012. (d) Kahn, O. *Chem. Phys. Lett.* **1997**, *265*, 109. (e) Bagai, R.; Abboud, K. A.; Christou, G. *Inorg. Chem.* **2007**, *46*, 5567. (f) Bagai, R.; Datta, S.; Betancur-Rodriguez, A.; Abboud, K. A.; Hill, S.; Christou, G. *Inorg. Chem.* **2007**, *46*, 4535.

(9) (a) Christou, G.; Gatteschi, D.; Hendrickson, D. N.; Sessoli, R. *MRS Bull.* **2000**, *25*, 66. (b) Gatteschi, D.; Sessoli, R. *Angew. Chem., Int. Ed.* **2003**, *42*, 268. (c) Bircher, R.; Chaboussant, G.; Dobe, C.; Güdel, H. U.; Ochsenbein, S. I.; Sieber, A.; Waldmann, O. *Adv. Funct. Mater.* **2006**, *16*, 209.

(10) For recent reviews, see:(a) Christou, G. *Polyhedron* **2005**, *24*, 2065. (b) Aromi, G.; Brechin, E. K. *Struct. Bonding (Berlin)* **2006**, *122*, 1.

(11) (a) Barra, A. L.; Caneschi, A.; Cornia, A.; de Biani, F. F.; Gatteschi, D.; Sangregorio, C.; Sessoli, R.; Sorace, L. *J. Am. Chem. Soc.* **1999**, *121*, 5302–5310.

(12) (a) Wieghardt, K.; Pohl, K.; Jibril, I.; Huttner, G. *Angew. Chem., Int. Ed. Engl.* **1984**, *23*, 77. (b) Delfs, C.; Gatteschi, D.; Pardi, L.; Sessoli, R.; Wieghardt, K.; Hanke, D. *Inorg. Chem.* **1993**, *32*, 3099.

(13) (a) Powell, G. W.; Lancashire, H. N.; Brechin, E. K.; Collison, D.; Health, S. L.; Mallah, T.; Wernsdorfer, W. *Angew. Chem., Int. Ed.* **2004**, *43*, 5772. (b) Bagai, R.; Wernsdorfer, W.; Abboud, K. A.; Christou, G. *J. Am. Chem. Soc.* **2007**, *129*, 12918.

(14) Goodwin, J. C.; Sessoli, R.; Gatteschi, D.; Wernsdorfer, D.; Powell, A. K.; Heath, S. L. *J. Chem. Soc., Dalton Trans.* **2000**, 1835.

(15) (a) Taft, K. L.; Delfs, C. D.; Papaefthymiou, G. C.; Foner, S.; Gatteschi, D.; Lippard, S. J. *J. Am. Chem. Soc.* **1994**, *116*, 823. (b) Mezei, G.; Baran, P.; Raptis, R. G. *Angew. Chem., Int. Ed.* **2004**, *43*, 573. (c) Normand, B.; Wang, X.; Zotos, X.; Loss, D. *Phys. Rev. B.* **2001**, *63*, 184409.

(16) (a) Kahn, O. *Molecular Magnetism*; VCH Publishers:New York, 1993. (b) Cornia, A.; Jansen, A. G. M.; Affronte, M.; Abbati, G. L.; Gatteschi, D. *Angew. Chem., Int. Ed.* **1999**, *38*, 2264. (c) Cornia, A.; Jansen, A. G. M.; Affronte, M. *Phys. Rev. B,* **1999**, *60*, 12177.

(17) (a) Chiolero, A.; Loss, D. *Phys. Rev. Lett.* **1998**, *80*, 169. (b) Meier, F.; Loss, D. *Phys. Rev. B.* **2001**, *64*, 224411. (c) Meier, F.; Loss, D. *Phys. Rev. Lett.* **2001**, *86*, 5373.

(18) Taft, K. L.; Lippard, S. J. *J. Am. Chem. Soc.* **1990**, *112*, 9629.

(19) (a) Benelli, C.; Parsons, S.; Solan, G. A.; Winpenny, R. E. P. *Angew. Chem., Int. Ed.* **1996**, *35*, 1825. (b) McInnes, E. J. L.; Anson, C.; Powell, A. K.; Thomson, A. J.; Poussereau, S.; Sessoli, R. *Chem. Commun.* **2001**, 89. (c) Helliwell, M.; Smith, A. A.; Teat, S. J.; Winpenny, R. E. P. *Inorg. Chim. Acta* **2003**, *354*, 49. (d) Cañada-Vilalta, C.; Pink, M.; Christou, G. *Chem. Commun.* **2003**, 1240. (e) Kooijman, H.; Spek, A. L.; Bouwman, E.; Micciche, F.; Warzeska, S. T.; Reedijk, J. *Acta Crystallogr., Sect. E* **2002**, *58*, m93. (f) Frey, M.; Harris, S. G.; Holmes, J. M.; Nation, D. A.; Parsons, S.; Tasker, P. A.; Teat, S. J.; Winpenny, R. E. P. *Angew. Chem., Int. Ed.* **1998**, *37*, 3246.

(20) For some representative examples, see:(a) Abbati, G. L.; Cornia, A.; Fabretti, A. C.; Malavasi, W.; Schenetti, L.; Caneschi, A.; Gatteschi, D. *Inorg. Chem.* **1997**, *36*, 6443. (b) Waldmann, O.; Schülein, J.; Koch, R.; Müller, P.; Bernt, I.; Saalfrank, R. W.; Andres, H. P.; Gudel, H. U.; Allenspach, P. *Inorg. Chem.* **1999**, *38*, 5879. (c) Saalfrank, R. W.; Bernt, I.; Chowdhry, M. M.; Hampel, F.; Vaughan, G. B. N. *Chem.—Eur. J.* **2001**, *7*, 2765. (d) Waldmann, O.; Koch, R.; Schromm, S.; Schülein, J.; Müller, P.; Bernt, I.; Saalfrank, R. W.; Hampel, F.; Balthes, E. *Inorg. Chem.* **2001**, *40*, 2986. (e) Jones, L. F.; Batsanov, A.; Brechin, E. K.; Collison, D.; Helliwell, M.; Mallah, T.; McInnes, E. J. L.; Piligkos, S. *Angew. Chem., Int. Ed.* **2002**, *41*, 4318. (f) Abu-Nawwas, A-A. H.; Cano, J.; Christian, P.; Mallah, T.; Rajaraman, G.; Teat, S. J.; Winpenny, R. E. P.; Yukawa, Y. *Chem. Commun.* **2004**, 314. (g) Lin, S.; Liu, S.- X.; Chen, Z.; Lin, B.- Z.; Gao, S. *Inorg. Chem.* **2004**, *43*, 2222.

(21) King, P.; Stamatatos, Th. C.; Abboud, K. A.; Christou, G. *Angew. Chem. Int. Ed* **2006**, *45*, 7379.

(22) Stamatatos, Th. C.; Christou, A. G.; Jones, C. M.; O'Callaghan, B. J.; Abboud, K. A.; O'Brien, T. A.; Christou, G. *J. Am. Chem. Soc.* **2007**, *129*, 9840.

to molecular wheels of different sizes and exploring both their intrinsic properties and their reactivity characteristics,[21,22] we have sought a convenient and high-yield route to Fe_{10} "ferric wheels" that would permit a fuller exploration of their chemistry. Such a route has now been successfully developed. We herein describe a general route to Fe_{10} "ferric wheels", their ready modification by carboxylate substitution and phenolysis, and their use as stepping-stones to Fe_2 and two Fe_8 clusters on reaction with ethylenediamine. We include a theoretical analysis of one of the Fe_8 complexes directed toward rationalizing its observed ground state *S* value.

Experimental Section

Syntheses. All manipulations were performed under aerobic conditions using chemicals and solvents as received. $[Fe_3O(O_2CR)_6(H_2O)_3]^+$ salts (R = Me, Et, Bu^t, Ph, etc) were synthesized as reported elsewhere;[23] "en" denotes ethylenediamine.

Safety Note. Caution! *Perchlorate salts are potentially explosive; such compounds should be synthesized and used in small quantities, and treated with utmost care at all times.*

$[Fe_{10}(OMe)_{20}(O_2CR)_{10}]$ (1): General Method. To a stirred orange-red solution of $[Fe_3O(O_2CR)_6(H_2O)_3](NO_3)$ (1.0 mmol) in MeOH (40 mL) was added NEt_3 (0.42 mL, 3.0 mmol). The resulting yellow slurry was stirred for 30−60 min, filtered, and the solid washed with cold MeOH (2 × 5 mL) and Et_2O (2 × 5 mL). Products at this stage were generally pure by elemental analysis. For recrystallization, the yellow microcrystalline residue was dissolved in CH_2Cl_2 (60 mL) or MeCN (60 mL) to give an essentially yellow solution, the solution was filtered, and the filtrate layered with Et_2O (120 mL). Yellow crystals began to appear within a few days. When crystallization was judged complete (10−12 days), the crystals were collected by filtration, washed with cold MeOH (2 × 5 mL) and Et_2O (2 × 5 mL), and dried under vacuum; the yields were typically ≥85%. Representative complex **1a** (R = Me) was characterized by X-ray crystallography, and the other analogues were identified by elemental analyses (C, H, N) and IR spectral comparison with **1a**. All the complexes are slightly moisture sensitive, and extensive exposure to air leads to progressive hydrolysis over many days to reddish-orange amorphous powders.

$[Fe_{10}(OMe)_{20}(O_2CMe)_{10}]$ (1a). This complex was structurally characterized by X-ray crystallography. It was prepared as described using $[Fe_3O(O_2CMe)_6(H_2O)_3](NO_3)$ (0.65 g, 1.0 mmol), and the washed yellow solid was recrystallized from MeCN/Et_2O (60/120 mL). Large yellow crystals of **1a**·10MeCN were collected by filtration, washed with cold MeCN (2 × 5 mL) and Et_2O (2 × 5 mL), and dried under vacuum; the yield was ∼85%. Anal. Calcd for **1a**·2MeCN: C, 28.54; H, 5.23; N, 1.51%. Found: C, 28.43; H, 5.27; N, 1.59%. Selected IR data (cm^{-1}): 3436 (mb), 2931 (m), 2824 (m), 1539 (s), 1438 (vs), 1043 (s), 669 (m), 539 (w), 454 (m), 413 (m).

$[Fe_{10}(OMe)_{20}(O_2CPh)_{10}]$ (1b). Method A. This complex was prepared as described using $[Fe_3O(O_2CPh)_6(H_2O)_3](NO_3)$ (1.03 g, 1.0 mmol). The yellow slurry was stirred for ∼30 min, filtered, and the yellow microcrystalline solid was washed with cold MeOH (2 × 5 mL) and Et_2O (2 × 5 mL), and dried under vacuum; the yield was ∼95%. Anal. Calcd for **1b** (solvent-free): C, 45.22; H, 4.64; N, 0.00%. Found: C, 45.33; H, 4.77; N, 0.00%. Selected IR data for **1b** (cm^{-1}): 3402 (mb), 2923 (m), 2819 (m), 1597 (s), 1523 (s), 1418 (vs), 1175 (m), 1041 (s), 938 (m), 838 (m), 718 (s), 680 (m), 581 (m), 474 (m).

Method B. Carboxylate Substitution. To a yellow solution of complex **1a** (1.77 g, 1.0 mmol) in a mixture of MeOH (50 mL) and CH_2Cl_2 (100 mL) was added $PhCO_2H$ (3.65 g, 30.0 mmol). The mixture was stirred for 1 h, and the solvent was then removed in vacuo. Toluene (20 mL) was added to the residue, and the solution was again evaporated to dryness. The addition and removal of toluene was repeated two more times. The remaining yellow solid was redissolved in CH_2Cl_2 (100 mL) and treated again with $PhCO_2H$ (3.65 g, 30.0 mmol). After 2 h, three more cycles of addition and removal of toluene were performed. The yellow residue was redissolved in CH_2Cl_2 (150 mL), filtered, layered with hexanes (80 mL), and maintained undisturbed at room temperature for 5 days. The resulting yellow crystals of **1b** were collected by filtration, washed with hexanes, and dried in vacuo; the yield was ∼90%. The identity of the product was confirmed by IR spectral comparison with material from Method A, and elemental analysis. Anal. Calcd for **1b** (solvent-free): C, 45.22; H, 4.64; N, 0.00%. Found: C, 45.39; H, 4.85; N, 0.00%.

Other Analogues. Anal. Calcd for **1c** (R = Et; solvent-free): C, 31.44; H, 5.81; N, 0.00%. Found: C, 31.31; H, 5.96; N, 0.02%. Selected IR data for **1c** (cm^{-1}): 3325 (mb), 2825 (m), 2814 (w), 1545 (s), 1430 (vs), 1042 (s), 671 (m), 555 (w), 539 (w), 457 (m), 419 (m). Anal. Calcd for **1d**·H_2O (R = Bu^t): C, 38.07; H, 6.94; N, 0.00%. Found: C, 37.95; H, 7.13; N, 0.02%. Selected IR data for **1d** (cm^{-1}): 3335 (mb), 2959 (m), 2945 (w), 2827 (m), 1543 (s), 1431 (vs), 1044 (s), 672 (m), 554 (w), 531 (w), 452 (m), 409 (m). Anal. Calcd for **1e**·$3H_2O$ (R = CH_2Bu^t): C, 40.29; H, 7.44; N, 0.00%. Found: C, 40.05; H, 7.59; N, 0.01%. Selected IR data for **1e** (cm^{-1}): 3333 (mb), 2961 (m), 2951 (m), 2942 (w), 2831 (m), 1544 (s), 1433 (vs), 1043 (s), 669 (m), 551 (w), 536 (w), 451 (m), 412 (m).

$[Fe_8(OH)_4(OPh)_8(O_2CBu^t)_{12}]$ (2). Method A. To a stirred yellow solution of $[Fe_{10}(OMe)_{20}(O_2CBu^t)_{10}]$ (1.1 g, 0.5 mmol) in CH_2Cl_2 (75 mL) was added a large excess of PhOH (1.41 g, 15.0 mmol). The resulting dark red solution was stirred for 1 h, filtered, and the filtrate layered with Et_2O (150 mL). After 2 days, large dark red crystals of **2**·H_2O·CH_2Cl_2 suitable for crystallography were collected by filtration, washed with CH_2Cl_2 (1 × 5 mL) and Et_2O (2 × 5 mL), and dried under vacuum; the yield was ∼30%. Anal. Calcd for **2** (solvent-free): C, 52.45; H, 6.19; N, 0.00%. Found: C, 52.27; H, 6.04; N, 0.09%. Selected IR data (cm^{-1}): 3422 (mb), 2964 (m), 1586 (m), 1540 (vs), 1494 (m), 1426 (s), 1370 (m), 1236 (m), 1177 (w), 1112 (w), 1024 (w), 836 (m), 788 (w), 680 (w), 602 (m), 491 (w), 442 (w).

Method B. To a stirred orange-red solution of $[Fe_3O(O_2CBu^t)_6(H_2O)_3](NO_3)$ (0.91 g, 1.0 mmol) in MeOH (20 mL) was added NEt_3 (0.42 mL, 3.0 mmol). The resulting yellow slurry was stirred for 15 min, during which time a colorless solution of PhOH (1.41 g, 15.0 mmol) in CH_2Cl_2 (60 mL) was added in portions. The resulting dark red solution was stirred for a further 1 h, filtered, and the filtrate layered with Et_2O (150 mL). After 4 days, dark red crystals were collected by filtration, washed with CH_2Cl_2 (1 × 5 mL) and Et_2O (2 × 5 mL), and dried under vacuum; the yield was ∼70%. The identity of the product was confirmed and IR spectral comparison with material from Method A, and by elemental analysis. Anal. Calcd for **2** (solvent-free): C, 52.45; H, 6.19; N, 0.00%. Found: C, 52.57; H, 6.12; N, 0.03%.

$[Fe_8O_5(O_2CMe)_8(en)_8](ClO_4)_6$ (3). Method A. To a stirred yellow solution of complex **1a** (0.89 g, 0.5 mmol) in MeCN (75

(23) (a) Duncan, J. F.; Kanekar, C. R.; Mok, K. F. *J. Chem. Soc., A* **1969**, *3*, 480. (b) Earnshaw, A.; Figgis, B. N.; Lewis, J. *J. Chem. Soc., A* **1966**, *12*, 1656. (c) Bond, A. M.; Clark, R. J. H.; Humphrey, D. G.; Panayiotopoulos, P.; Skelton, B. W.; White, A. H. *J. Chem. Soc., Dalton Trans.* **1998**, *11*, 1845.

Table 1. Crystallographic Data for **1a**·10MeCN, **2**·H_2O·CH_2Cl_2, **3**·8MeCN, and **4**

Parameter	1a	2	3	4
formula[a]	$C_{60}H_{120}N_{10}O_{40}Fe_{10}$	$C_{109}H_{156}O_{37}Cl_2Fe_8$	$C_{48}H_{112}N_{24}O_{45}Cl_6Fe_8$	$C_{13}H_{33}N_{11}O_{12}Fe_2$
fw, g mol^{-1}[a]	2180.17	2576.14	2405.08	647.17
crystal system	monoclinic	monoclinic	trigonal	orthorhombic
space group	$P2_1/c$	$P2_1/n$	$P3_2$	*Pnma*
α, Å	17.4670(13)	16.2838(15)	14.4754(14)	8.8351(6)
b, Å	33.037(2)	19.0907(17)	14.4754(14)	11.5547(8)
c, Å	15.2524(11)	21.756(2)	40.569(9)	27.7279(18)
β, deg	93.117(2)	103.609(2)	90	90
V, $Å^3$	8788.4(1)	6573.4(1)	7362.0(2)	2830.7(3)
Z	4	2	3	4
T, °C	173(2)	173(2)	173(2)	173(2)
radiation, Å[b]	0.71073	0.71073	0.71073	0.71073
ρ_{calc}, g cm^{-3}	1.648	1.301	1.617	1.538
μ, mm^{-1}	1.691	0.968	1.407	1.097
*R*1[c,d]	0.0641	0.0568	0.0936	0.0336
*wR*2[e]	0.1554	0.1404	0.1852	0.0824

[a] Including solvate molecules. [b] Graphite monochromator. [c] $I > 2\sigma(I)$. [d] $R1 = \sum(||F_o| - |F_c||)/\sum|F_o|$. [e] $wR2 = [\sum[w(F_o^2 - F_c^2)^2]/\sum[w(F_o^2)^2]]^{1/2}$, $w = 1/[\sigma^2(F_o^2) + [(ap)^2 + bp]$, where $p = [\max(F_o^2, 0) + 2F_c^2]/3$.

mL) was added an excess of en (0.30 g, 5.0 mmol). The resulting dark red solution was stirred for 3 h, during which time solid $NaClO_4$·H_2O (0.42 g, 3.0 mmol) was added in portions. During this time, the color of the solution also changed to dark green. After a further 10 min, the solution was filtered, and the filtrate layered with Et_2O (150 mL). After 10 days, large dark green crystals of **3**·8MeCN suitable for crystallography were collected by filtration, washed with cold MeCN (2 × 5 mL) and Et_2O (2 × 5 mL), and dried under vacuum; the yield was ∼20%. Anal. Calcd. for **3**·3MeCN: C, 20.75; H, 4.44; N, 12.10%. Found: C, 20.67; H, 4.37; N, 12.19%. Selected IR data (cm^{-1}): 3337 (s), 2961 (m), 2900 (w), 1585 (m), 1514 (m), 1416 (m), 1338 (w), 1278 (w), 1078 (vs), 1033 (s), 975 (m), 795 (m), 655 (m), 623 (s), 510 (m), 424 (w).

Method B. To a stirred orange-red solution of $[Fe_3O(O_2CMe)_6(H_2O)_3](NO_3)$ (0.65 g, 1.0 mmol) in MeOH (20 mL) was added NEt_3 (0.42 mL, 3.0 mmol). The resulting yellow slurry was stirred for 15 min, during which time a solution of en (0.18 g, 3.0 mmol) in MeCN (30 mL) was added in small portions. The resulting dark red solution was treated with an excess of solid $NaClO_4$·H_2O (0.84 g, 6.0 mmol), and stirred for a further 1 h, after which it was evaporated to dryness under reduced pressure. The residue was redissolved in MeCN (50 mL) to give a dark green solution, and this was filtered and layered with Et_2O (100 mL). After 4 days, large dark green crystals were collected by filtration, washed with cold MeCN (2 × 5 mL) and Et_2O (2 × 5 mL), and dried under vacuum; the yield was ∼60%. The identity of the product was confirmed by IR spectral comparison with material from Method A, and elemental analysis. Anal. Calcd. for **3**·6MeCN: C, 22.75; H, 4.60; N, 13.27%. Found: C, 22.46; H, 4.51; N, 13.39%.

$[Fe_2O(O_2CBu^t)(en)_4](NO_3)_3$ (4). Method A. To a stirred yellow solution of $[Fe_{10}(OMe)_{20}(O_2CBu^t)_{10}]$ (1.10 g, 0.5 mmol) in dimethylformamide (DMF, 35 mL) was added an excess of en (0.30 g, 5.0 mmol). The resulting dark red solution was stirred for a further 2 h, during which time solid $NaNO_3$ (0.26 g, 3.0 mmol) was added in portions; the color of the solution slowly changed to dark green. After a further 20 min, the solution was filtered, and the filtrate layered with Et_2O (70 mL). After 7 days, large dark green crystals of **4** suitable for crystallography were collected by filtration, washed with DMF (1 × 5 mL) and Et_2O (2 × 5 mL), and dried under vacuum; the yield was ∼10%. Anal. Calcd for **4** (solvent-free): C, 23.83; H, 6.31; N, 23.51%. Found: C, 24.22; H, 6.68; N, 23.46%. Selected IR data (cm^{-1}): 3420 (mb), 2962 (m), 1658 (m), 1578 (m), 1522 (m), 1384 (vs), 1279 (w), 1227 (w), 1158 (w), 1107 (w), 1039 (m), 825 (m), 788 (m), 668 (m), 607 (m), 517 (m), 426 (w).

Method B. To a stirred orange-red solution of $Fe(NO_3)_3$·$9H_2O$ (0.81 g, 2.0 mmol) in DMF (20 mL) was added solid NaO_2CBu^t (0.12 g, 1.0 mmol). The resulting dark red solution was stirred for 15 min, during which time a colorless solution of en (0.24 g, 4.0 mmol) and NEt_3 (0.07 mL, 0.5 mmol) in DMF (30 mL) was added in small portions. The dark red solution was stirred for a further 1 h, during which time the color changed to dark green. The solution was then filtered, and the filtrate layered with Et_2O (100 mL). After 2 days, large dark green crystals were collected by filtration, washed with cold DMF (1 × 5 mL) and Et_2O (2 × 5 mL), and dried under vacuum; the yield was ∼80%. The identity of the product was confirmed by IR spectral comparison with material from Method A, and elemental analysis. Anal. Calcd for **4** (solvent-free): C, 23.83; H, 6.31; N, 23.51%. Found: C, 24.05; H, 6.54; N, 23.47%.

X-ray Crystallography. Data were collected on a Siemens SMART PLATFORM equipped with a CCD area detector and a graphite monochromator utilizing Mo Kα radiation ($\lambda = 0.71073$ Å). Suitable crystals of **1a**·10MeCN, **2**·H_2O·CH_2Cl_2, **3**·8MeCN, and **4** were attached to glass fibers using silicone grease and transferred to a goniostat where they were cooled to 173 K for data collection. An initial search of reciprocal space revealed a monoclinic cell for **1a**·10MeCN and **2**·H_2O·CH_2Cl_2, a trigonal cell for **3**·8MeCN, and an orthorhombic cell for **4**; the choices of space groups $P2_1/c$ (for **1a**·10MeCN), $P2_1/n$ (for **2**·H_2O·CH_2Cl_2), $P3_2$ (for **3**·8MeCN), and *Pnma* (for **4**) were confirmed by the subsequent solution and refinement of the structures. Cell parameters were refined using up to 8192 reflections. A full sphere of data (1850 frames) was collected using the *ω*-scan method (0.3° frame width). The first 50 frames were remeasured at the end of data collection to monitor instrument and crystal stability (maximum correction on *I* was <1%). Absorption corrections by integration were applied based on measured indexed crystal faces. The structures were solved by direct methods in SHELXTL6,[24] and refined on F^2 using full-matrix least-squares. The non-H atoms were treated anisotropically, whereas the H atoms were placed in calculated, ideal positions and refined as riding on their respective C atoms. Unit cell parameters and structure solution and refinement data are listed in Table 1.

For **1a**·10MeCN, the asymmetric unit consists of the complete Fe_{10} cluster, and ten disordered MeCN molecules of crystallization. The latter could not be modeled properly, thus the program

(24) *SHELXTL6*; Bruker-AXS: Madison, WI, 2000.

SQUEEZE,[25] a part of the PLATON package of crystallographic software, was used to calculate the solvent disorder area and remove its contribution to the overall intensity data. A total of 811 parameters were included in the structure refinement using 18911 reflections with $I > 2\sigma(I)$ to yield R_1 and wR_2 of 6.41 and 15.54%, respectively. For **2**·H_2O·CH_2Cl_2, the asymmetric unit consists of half-the Fe_8 cluster, and half-each of H_2O and CH_2Cl_2 molecules of crystallization disordered about an inversion center. The program SQUEEZE[25] was again used to calculate the solvent disorder area and remove its contribution to the overall intensity data. A total of 595 parameters were included in the structure refinement using 7966 reflections with $I > 2\sigma(I)$ to yield R_1 and wR_2 of 5.68 and 14.04%, respectively. For **3**·8MeCN, the asymmetric unit consists of the complete Fe_8 cluster, six ClO_4^- anions, and eight MeCN molecules of crystallization, which were badly disordered and again treated with the program SQUEEZE.[25] A total of 597 parameters were included in the structure refinement using 4372 reflections with $I > 2\sigma(I)$ to yield R_1 and wR_2 of 9.36 and 18.52%, respectively. For **4**, the asymmetric unit consists of half the Fe_2 molecule, and one and a half NO_3^- anions; there were no molecules of crystallization in the lattice. A total of 231 parameters were included in the structure refinement using 3136 reflections with $I > 2\sigma(I)$ to yield R_1 and wR_2 of 3.36 and 8.24%, respectively.

Physical Measurements. Infrared spectra were recorded in the solid state (KBr pellets) on a Nicolet Nexus 670 FTIR spectrometer in the 400−4000 cm^{-1} range. Elemental analyses (C, H, and N) were performed by the in-house facilities of the University of Florida Chemistry Department. Variable-temperature direct current (dc) and alternating current (ac) magnetic susceptibility data were collected at the University of Florida using a Quantum Design MPMS-XL SQUID susceptometer equipped with a 7 T magnet and operating in the 1.8−300 K range. Samples were embedded in solid eicosane to prevent torquing. Pascal's constants were used to estimate the diamagnetic corrections, which were subtracted from the experimental susceptibilities to give the molar paramagnetic susceptibilities (χ_M).

Theoretical Calculations. ZILSH calculations were performed on the large cluster **3**. According to the ZILSH procedure,[26] unrestricted Hartree−Fock (UHF) wave functions are obtained with the INDO/S method of Zerner[27] for spin components in which the spins of certain metals are reversed relative to the others. The energies are assumed to follow an effective Heisenberg formula given in eq 1,

$$E_i = E_0 - \sum_{A<B} 2J_{AB}\langle \hat{S}_A \cdot \hat{S}_B \rangle^{UHF} \quad (1)$$

where i labels the spin component and E_0 contains all spin-independent contributions to the energy. Spin couplings $\langle \hat{S}_A \cdot \hat{S}_B \rangle^{UHF}$ (A, B label metal ions) appearing in eq 1 are obtained with the local spin operator of Davidson et al.[28] Given the energies and spin couplings for a sufficient number of components, multiple eqs 1 can be solved simultaneously for E_0 and the exchange constants J_{AB}. The spin components used for **3** were the component with all unpaired spins aligned parallel and with all the components with unpaired spins of two metals antiparallel to the other unpaired spins. This provides the appropriate number of components for solving eq 1 for all pairwise exchange constants in each case. The ZILSH calculations also both provide the local spin density M_i for each metal ion, which equals the number of unpaired electrons associated with that ion.[26] This quantity indicates if the correct oxidation states and metal d electron configurations were obtained for the metal ions.

Given exchange constants obtained as just described, wave functions and energies for the spin eigenstates of a complex can be found by substituting the exchange constants into the Heisenberg spin Hamiltonian. The operator is then diagonalized in a basis of spin components $\phi_i = |m_1\ m_2\ \cdots\ m_N\rangle_i$, where m_A is a formal value of the local z component of the spin of metal "A" ($m_A = {}^5/_2, {}^3/_2, {}^1/_2, -{}^1/_2, -{}^3/_2, -{}^5/_2$ for high-spin Fe^{3+} ions). The resulting spin eigenstate wave functions are then linear combinations of these components (eq 2), where the expansion

$$|\psi_S\rangle = \sum_i C_i \varphi_i \quad (2)$$

runs over components for which the local z components of spin add to the total spin S of the state. Given the large size of the complexes involved, the energy and wave function for the lowest energy state of each spin were obtained with the Davidson algorithm[29] rather than by diagonalizing the entire Heisenberg matrix.

One important quantity that can be calculated from the wave functions is the spin coupling $\langle \hat{S}_A \cdot \hat{S}_B \rangle$ for each pair of metal ions. These values are useful for identifying exchange pathways that are spin frustrated.[30,31] The spin coupling indicates the true alignment of z components m_A and m_B in the state, while the exchange constant J_{AB} indicates the preferred alignment. Any pathway with $\langle \hat{S}_A \cdot \hat{S}_B \rangle$ and J_{AB} of different signs is thus frustrated under the $-2J$ convention. This is used to describe the spin interactions in the ground state of **3** given its complicated core structure consisting of triangular motifs, which often lead to spin frustration (vide infra).

Results and Discussion

Syntheses. The triangular $[Fe_3O(O_2CR)_6(L)_3]^+$ species have proven on numerous occasions to be excellent stepping-stones to new polynuclear species. Most of these reactions have been with a potentially chelating or similar reagent, and high-nuclearity products have included $[Fe_{14}O_4(O_2)_2(O_2CBu^t)_{12}(O_3PPh)_8(H_2O)_{12}]^{2+}$,[32] $[Fe_{16}(OEt)_4(O_2CPh)_{16}(thmeH)_{12}]^{4+}$,[20e] $[Fe_{18}O_8(OH)_2(O_2CBu^t)_{28}(heen)_4]$,[33] and $[Fe_{22}O_{14}(OH)_3(O_2CMe)_{21}(mda)_6]^{2+}$.[34] In such reactions, the $[Fe_3O]^{7+}$ core of the starting material serves as a building block for higher nuclearity products, but their exact nuclearity and structure still depend on factors such as the carboxylate group, the reaction solvent, the pH of the solution, and others. With only carboxylate peripheral ligands, however, only a very few high-nuclearity Fe(III) clusters have been isolated

(25) Van der Sluis, P.; Spek, A. L. *Acta Crystallogr., Sect. A: Found. Crystallogr.* **1990**, *A46*, 194.
(26) O'Brien, T. A.; Davidson, E. R. *Int. J. Quantum Chem.* **2003**, *92*, 294.
(27) Zerner, M. C.; Loew, G. H.; Kirchner, R. F.; Mueller-Westerhoff, U. T. *J. Am. Chem. Soc.* **1980**, *102*, 589.
(28) Clark, A. E.; Davidson, E. R. *J. Chem. Phys.* **2001**, *115*, 7382.
(29) Davidson, E. R. *J. Comput. Phys.* **1975**, *17*, 87.
(30) (a) Cañada-Vilalta, C.; O'Brien, T. A.; Pink, M.; Davidson, E. R.; Christou, G. *Inorg. Chem.* **2003**, *42*, 7819; and references therein. (b) Cañada-Vilalta, C.; O'Brien, T. A.; Brechin, E. K.; Pink, M.; Davidson, E. R.; Christou, G. *Inorg. Chem.* **2004**, *43*, 5505.
(31) O'Brien, T. A.; O'Callaghan, B. J. *J. Chem. Theory Comput.* **2007**, *3*, 1275.
(32) Tolis, E. I.; Helliwell, M.; Langley, S.; Raftery, J.; Winpenny, R. E. P. *Angew. Chem., Int. Ed.* **2003**, *42*, 3804.
(33) Bagai, R.; Abboud, K. A.; Christou, G. *Chem. Commun.* **2007**, 3359.
(34) Foguet-Albiol, D.; Abboud, K. A.; Christou, G. *Chem. Commun.* **2005**, 4282.

to date, namely $[Fe_{11}O_6(OH)_6(O_2CPh)_{15}]$[35] and $[Fe_{17}O_{10}(OH)_{10}(O_2CPh)_{20}]$,[36] which were obtained by hydrolysis. It thus seemed to us that the triangular $[Fe_3O(O_2CR)_6(L)_3]^+$ complexes might also provide the desired high yield routes to the ferric wheel complexes from methanolysis reactions under the right conditions, namely basic ones. Preliminary experimentation soon showed this to be the case.

The reaction of $[Fe_3O(O_2CR)_6(H_2O)_3]^+$ salts with NEt_3 in a 1:3 molar ratio in MeOH rapidly gave yellow slurries and the subsequent isolation of yellow microcrystalline solids that proved to be the "ferric wheel" complexes $[Fe_{10}(OMe)_{20}(O_2CR)_{10}]$ (**1**) (R = Me (**1a**), Ph (**1b**), etc) in excellent yields (>85%) and high purity even before recrystallization. The preparation of **1** is summarized in eq 3.

$$10[Fe_3O(O_2CR)_6(H_2O)_3]^+ + 40NEt_3 + 60MeOH \rightarrow 3[Fe_{10}(OMe)_{20}(O_2CR)_{10}] + 30RCO_2^- + 40NHEt_3^+ + 40H_2O \quad (3)$$

Doubling of the amount of NEt_3 again gave **1** in the same yields, whereas there was no apparent reaction in the absence of NEt_3.

Reactivity Studies. The availability of large quantities of complex **1** has allowed a variety of detailed reactivity studies on ferric wheels for the first time, which we shall describe as three groups.

(A) Ligand Substitution. Carboxylate substitution with benzoic acid has been investigated on **1a** in $MeOH/CH_2Cl_2$. Such substitution reactions are with precedent in metal carboxylate cluster chemistry, such as in the replacement of the acetates of $[Mn_{12}O_{12}(O_2CMe)_{16}(H_2O)_4]$ with essentially any carboxylate of choice, opening up access to a large family of Mn_{12} derivatives.[37] The substitution is an equilibrium that must be driven to completion by (i) using a carboxylic acid with a lower pK_a than that of acetic acid (4.76), and/or (ii) using an excess of $PhCO_2H$, and/or (iii) removing the acetic acid as its toluene azeotrope (28:72%; bp 101 °C at 1 atmosphere). With **1a**, we used all three of these conditions, employing an excess (30 equiv) of $PhCO_2H$ (pK_a = 4.20)[38] and carrying out multiple cycles of addition and removal of toluene under dynamic vacuum to remove acetic acid. Our main worry was that the excess of $PhCO_2H$ would protonate the bridging methoxide groups causing degradation of the wheel, perhaps back to $[Fe_3O(O_2CPh)_6(H_2O)_3]^+$, but the carboxylate substitution was instead found to proceed cleanly to give pure $[Fe_{10}(OMe)_{20}(O_2CPh)_{10}]$ (**1b**) in nearly quantitative isolated yield (~90%). The preparation is summarized in eq 4.

$$[Fe_{10}(OMe)_{20}(O_2CMe)_{10}] + 10PhCO_2H \rightarrow [Fe_{10}(OMe)_{20}(O_2CPh)_{10}] + 10MeCO_2H \quad (4)$$

The same method was employed with $ClCH_2CO_2H$ (pK_a = 2.87)[38] instead of $PhCO_2H$ and gave $[Fe_{10}(OMe)_{20}(O_2CCH_2Cl)_{10}]$ in ~80% isolated yield.

In contrast, we were unable to achieve clean alcohol substitution of the bridging MeO^- groups with EtOH to generate the corresponding $[Fe_{10}(OEt)_{20}(O_2CR)_{10}]$ complexes, even when we carried out the initial preparation in neat EtOH instead of MeOH. All isolated yellow solids analyzed as mixed OEt^-/OH^- species, namely, $[Fe_{10}(OH)_x(OEt)_{20-x}(O_2CR)_{10}]$. For example, the R = Me and Ph products analyzed with x = 10 and 14, respectively. The greater susceptibility of the ethoxide products to hydrolysis might be simply due to the greater basicity of EtO^- versus MeO^-, as reflected in the relative pK_a values for EtOH and MeOH of 15.9 and 15.5, respectively. Similarly mixed-bridged products but involving MeO^-/EtO^- have been reported in "chromic wheel" complexes such as $[Cr_{10}(OMe)_{10}(OEt)_{10}(O_2CMe)_{10}]$.[39]

(B) Phenolysis Reactions. As an extension to the alcohol substitution attempts above, we explored reactions with PhOH (pK_a = 9.98), which is both more acidic and bulkier than MeOH. In this case, complete alkoxide substitution readily occurred but also a change in the wheel nuclearity. Thus, addition of a large excess of PhOH to $[Fe_{10}(OMe)_{20}(O_2CBu^t)_{10}]$ in CH_2Cl_2 gave a dark red solution from which were subsequently isolated dark red crystals of $[Fe_8(OH)_4(OPh)_8(O_2CBu^t)_{12}]$ (**2**) in ~30% yield based on Fe. The phenolysis reaction is summarized in eq 5.

$$6[Fe_{10}(OMe)_{20}(O_2CBu^t)_{10}] + 100PhOH + 20H_2O \rightarrow 5[Fe_8(OH)_4(OPh)_8(O_2CBu^t)_{12}] + 20\text{ ``}Fe(OPh)_3\text{''} + 120MeOH \quad (5)$$

Complex **2** is also a wheel (vide infra) but its decreased Fe/$Bu^tCO_2^-$ ratio shows that its formation is not simply a MeO^-/PhO^- exchange followed by wheel contraction. Thus, the yield is carboxylate-limited and actually ~45% on this basis. The reaction of $[Fe_{10}(OMe)_{20}(O_2CPh)_{10}]$ with PhOH proceeded analogously to give $[Fe_8(OH)_4(OPh)_8(O_2CBu^t)_{12}]$, which has been previously reported resulting from a very different procedure.[30a] Similar products were also obtained with 4-*tert*-butylphenol and 3,5-di-*tert*-butylphenol, as confirmed by elemental analysis (C, H, N), IR spectroscopy, and a partial X-ray crystallographic characterization for the former.

Complex **2** was also obtained directly from $[Fe_3O(O_2CBu^t)_6(H_2O)_3](NO_3)$ in $MeOH/CH_2Cl_2$ by treatment with 3 equiv of NEt_3, to generate the Fe_{10} wheel *in situ*, followed by addition of a large excess of PhOH (Method B). This gave a yield of ~70% based on Fe, much higher than that

(35) Gorun, S. M.; Papaefthymiou, G. C.; Frankel, R. B.; Lippard, S. J. *J. Am. Chem. Soc.* **1987**, *109*, 3337.
(36) Micklitz, W.; McKee, V.; Rardin, L.; Pence, L. E.; Papaefthymiou, G. C.; Bott, S. M.; Lippard, S. J. *J. Am. Chem. Soc.* **1994**, *116*, 8061.
(37) (a) Sessoli, R.; Tsai, H.-L.; Schake, A. R.; Wang, S.; Vincent, J. B.; Folting, K.; Gatteschi, D.; Christou, G.; Hendrickson, D. N. *J. Am. Chem. Soc.* **1993**, *115*, 1804. (b) Sessoli, R.; Gatteschi, D.; Caneschi, A.; Novak, M. A. *Nature* **1993**, *365*, 141. (c) Artus, P.; Boskovic, C.; Yoo, Y.; Streib, W. E.; Brunel, L.-C.; Hendrickson, D. N.; Christou, G. *Inorg. Chem.* **2001**, *40*, 4199. (d) Soler, M.; Artus, P.; Folting, K.; Huffman, J. C.; Hendrickson, D. N.; Christou, G. *Inorg. Chem.* **2001**, *40*, 4902. (e) Chakov, N. E.; Lee, S.- C.; Harter; Kuhns, P. L.; Reyes, A. P.; Hill, S. O.; Dalal, N. S.; Wernsdorfer, W.; Abboud, K. A.; Christou, G. *J. Am. Chem. Soc.* **2006**, *128*, 6975.
(38) *Tables for Organic Compound Identification*; Rappoport, Z., Ed.; CRC Press: Cleveland, OH, 1967.
(39) Sun, L.; Zhang, J.; Cui, S. *Polyhedron* **2007**, *26*, 2169.

from Method A. The phenolysis reactions were also performed in the presence of NBu^n_4X (X = Cl^-, Br^-) with the aim of replacing the guest water molecule in the central cavity (vide infra) with X^-, perhaps resulting in a larger Fe_x ($x > 8$) wheel, but the isolated product was again complex **2**.

(C) Reactions with Ethylenediamine (en). The use of ferric wheels as starting materials in reactions with a bidentate chelate was expected to unavoidably lead to structural transformation. We chose en, whose Fe cluster chemistry has so far been limited to the Fe^{II} cluster $[Fe_5(OH)_2(O_2CPh)_6(en)_4]^{2+}$.[40] The reaction between 10 equiv of en and **1a** in MeCN containing $NaClO_4$ led to a dark green solution from which well-formed green crystals of $[Fe_8O_5(O_2CMe)_8(en)_8](ClO_4)_6$ (**3**) were obtained in fair yields (~20%). The formation of **3** is summarized in eq 6.

$$4[Fe_{10}(OMe)_{20}(O_2CMe)_{10}] + 40en + 55H_2O \rightarrow 5[Fe_8O_5(O_2CMe)_8(en)_8]^{6+} + 80MeOH + 30OH^- \quad (6)$$

Again, a much higher yield (~60%) was obtained when the Fe_{10} wheel was generated *in situ* from $[Fe_3O(O_2CMe)_6(H_2O)_3](NO_3)$ and 3 equiv of NEt_3 in MeOH, and then treated with 3 equiv of en in MeCN (Method B). Increasing the amount of NEt_3 or en still gave complex **3** but in lower yields and contaminated with other products.

In contrast to the above, the $[Fe_{10}(OMe)_{20}(O_2CBu^t)_{10}]$, en, and $NaNO_3$ (1:10:6) reaction in DMF (Method A) gave the dinuclear $[Fe_2O(O_2CBu^t)(en)_4](NO_3)_3$ (**4**) in poor yield (~10%) (eq 7).

$$[Fe_{10}(OMe)_{20}(O_2CBu^t)_{10}] + 20en + 15H_2O \rightarrow 5[Fe_2O(O_2CBu^t)(en)_4]^{3+} + 5Bu^tCO_2^- + 20MeOH + 10OH^- \quad (7)$$

However, a much higher yield procedure (80%) was again developed once the identity of **4** had been established employing the $Fe(NO_3)_3$, NaO_2CBu^t, en, and NEt_3 (4:2:8:1) reaction in DMF (Method B). Note that the excess en can also function as a base in these reactions, as well as the NEt_3 and MeO^-, facilitating the formation of oxide ions. Complex **4** could also be obtained in other reaction solvents (MeCN or CH_2Cl_2), but the yields were appreciably lower and the product was contaminated with some white solid.

Description of Structures. The structure of complex **1a** is shown in Figure 1. The structure is essentially identical to previously characterized Fe_{10} ferric wheels[18−20] and is thus only briefly discussed. The Fe_{10} molecule has virtual D_{5d} symmetry and comprises a near-planar (±0.009−0.052 Å) wheel of ten octahedral Fe^{III} atoms with each Fe_2 pair bridged by one $MeCO_2^-$ and two MeO^- groups, giving layers of O atoms above and below the Fe_{10} wheel (Figure 1, middle). The space-filling view of Figure 1, bottom, reveals a small central hole of ~3 Å diameter unoccupied by any guest molecule. The Fe_{10} molecules pack in the crystal on top of each other forming supramolecular nanotubular stacks parallel to the *c* axis.

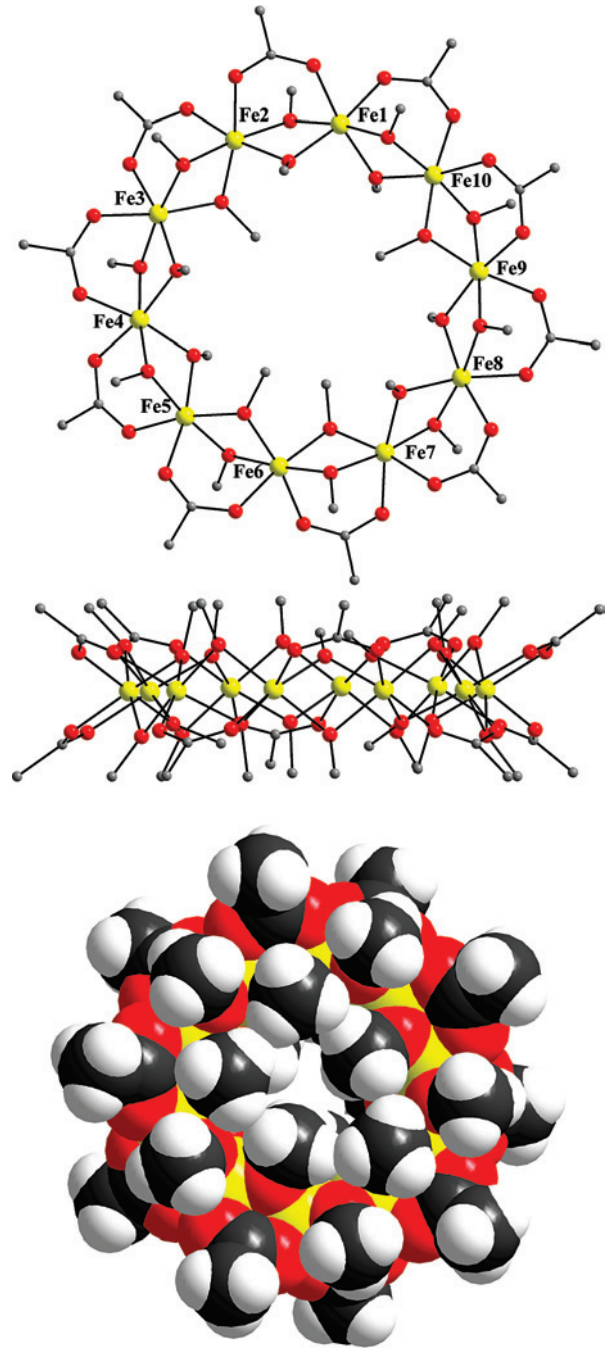

Figure 1. (top) Labeled PovRay representation of the structure of **1a**, with the hydrogen atoms omitted for clarity; (middle) side-view emphasizing the wheel planarity and O/Fe/O layered structure; (bottom) space-filling representation. Color code: Fe, yellow; O, red; C, gray; H, white.

An Oak Ridge Thermal Ellipsoid Plot (ORTEP) representation of complex **2** is shown in Figure 2. The structure is similar to that previously reported.[30a] The molecule has crystallographic C_i and virtual D_{4d} symmetry and consists of a planar wheel of eight Fe(III) ions with alternating Fe_2 pairs bridged by $(\mu\text{-}O_2CBu^t)(\mu\text{-}OPh)_2$ and $(\mu\text{-}OH)(\mu\text{-}O_2CBu^t)_2$ ligand sets, resulting in distinctly different Fe···Fe separations of 3.096−3.104 and 3.423−3.455 Å, respectively. There is a central H_2O guest molecule at the center

(40) Lachicotte, R. J.; Hagen, K. S. *Inorg. Chim. Acta* **1997**, *263*, 407.

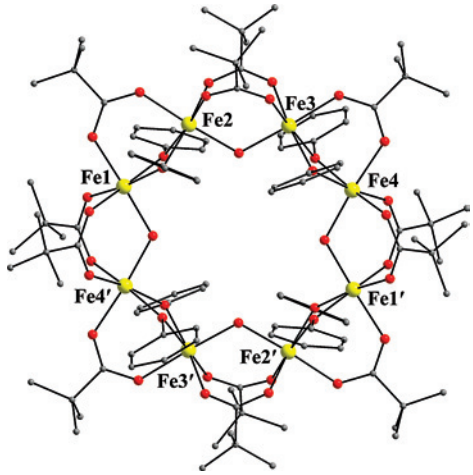

Figure 2. Labeled PovRay representation of the structure of **2**, with the hydrogen atoms omitted for clarity. Color code: Fe, yellow; O, red; C, gray.

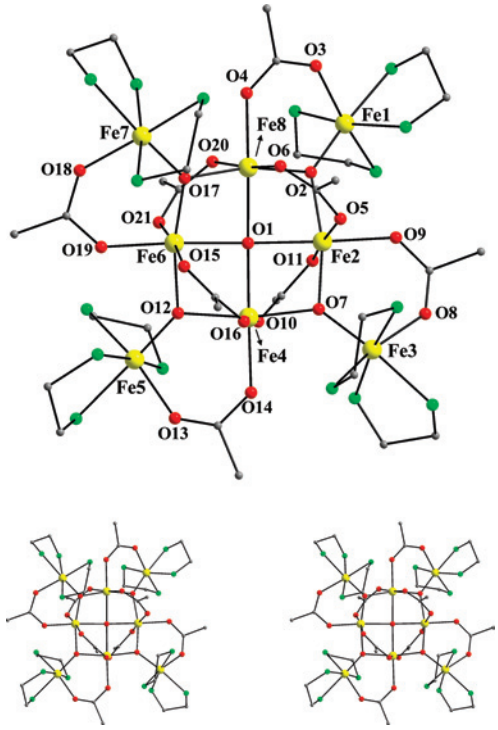

Figure 3. PovRay representation (top) and stereoview (bottom) of the structure of **3**, with the hydrogen atoms omitted for clarity. Color code: Fe, yellow; O, red; N, green; C, gray.

of the wheel, hydrogen-bonded to the bridging OH^- ions and disordered in two positions above and below the Fe_8 plane.

The partially labeled structure and a stereoview of the $[Fe_8O_5(O_2CMe)_8(en)_8]^{6+}$ cation of **3** are shown in Figure 3, and selected interatomic distances and angles are listed in Table 2. Complex **3** crystallizes in the trigonal space group $P3_2$ with the Fe_8 molecule in a general position. The cation thus has crystallographic C_1 but virtual S_4 symmetry, and consists of a central planar $[Fe_4(\mu_4\text{-}O^{2-})]$ square (Fe2, Fe4, Fe6, Fe8) whose four edges are each fused with the edge of a $[Fe_3(\mu_3\text{-}O^{2-})]$ triangle. The resulting $[Fe_8(\mu_4\text{-}O)(\mu_3\text{-}O)_4]^{14+}$ core has a "Christmas-star" topology (Figure 4). The central $\mu_4\text{-}O^{2-}$ O1 atom has very rare square-planar geometry, which

Table 2. Selected Interatomic Distances (Å) and Angles (deg) for **3**·8MeCN

parameter		parameter	
Fe(1)−O(2)	1.818(1)	Fe(5)−O(12)	1.859(2)
Fe(1)−O(3)	2.043(3)	Fe(5)−O(13)	2.049(2)
Fe(1)−N(1)	2.164(2)	Fe(5)−N(9)	2.131(2)
Fe(1)−N(2)	2.105(2)	Fe(5)−N(10)	2.192(2)
Fe(1)−N(3)	2.243(2)	Fe(5)−N(11)	2.128(2)
Fe(1)−N(4)	2.098(2)	Fe(5)−N(12)	2.070(2)
Fe(2)−O(1)	2.032(1)	Fe(6)−O(1)	2.077(1)
Fe(2)−O(2)	2.025(1)	Fe(6)−O(12)	1.946(2)
Fe(2)−O(5)	2.090(1)	Fe(6)−O(15)	2.142(1)
Fe(2)−O(7)	1.851(1)	Fe(6)−O(17)	1.915(1)
Fe(2)−O(9)	1.978(1)	Fe(6)−O(19)	1.993(1)
Fe(2)−O(11)	2.077(1)	Fe(6)−O(21)	2.045(1)
Fe(3)−O(7)	1.862(1)	Fe(7)−O(17)	1.869(1)
Fe(3)−O(8)	2.002(2)	Fe(7)−O(18)	1.972(2)
Fe(3)−N(5)	2.144(2)	Fe(7)−N(13)	2.184(2)
Fe(3)−N(6)	2.172(2)	Fe(7)−N(14)	2.143(2)
Fe(3)−N(7)	2.085(2)	Fe(7)−N(15)	2.123(2)
Fe(3)−N(8)	2.250(2)	Fe(7)−N(16)	2.204(2)
Fe(4)−O(1)	2.034(1)	Fe(8)−O(1)	2.040(1)
Fe(4)−O(7)	1.993(1)	Fe(8)−O(2)	1.889(1)
Fe(4)−O(10)	2.050(1)	Fe(8)−O(4)	2.033(1)
Fe(4)−O(12)	1.908(2)	Fe(8)−O(6)	2.056(1)
Fe(4)−O(14)	2.009(1)	Fe(2)−O(17)	1.926(1)
Fe(4)−O(16)	2.027(1)	Fe(8)−O(20)	2.056(1)
Fe(1)···Fe(2)	3.528(7)	Fe(4)···Fe(5)	3.379(8)
Fe(1)···Fe(8)	3.382(8)	Fe(4)···Fe(6)	2.882(4)
Fe(2)···Fe(3)	3.368(5)	Fe(4)···Fe(8)	4.074(7)
Fe(2)···Fe(4)	2.894(9)	Fe(5)···Fe(6)	3.523(7)
Fe(2)···Fe(6)	4.109(7)	Fe(6)···Fe(7)	3.365(4)
Fe(2)···Fe(8)	2.890(4)	Fe(6)···Fe(8)	2.907(9)
Fe(3)···Fe(4)	3.523(6)	Fe(7)···Fe(8)	3.518(5)
Fe(1)−O(2)−Fe(2)	133.2(7)	Fe(4)−O(1)−Fe(6)	89.0(6)
Fe(1)−O(2)−Fe(8)	131.7(7)	Fe(4)−O(1)−Fe(8)	178.3(7)
Fe(2)−O(1)−Fe(4)	90.7(5)	Fe(4)−O(12)−Fe(5)	127.5(8)
Fe(2)−O(1)−Fe(6)	178.9(6)	Fe(4)−O(12)−Fe(6)	96.8(7)
Fe(2)−O(1)−Fe(8)	90.4(6)	Fe(5)−O(12)−Fe(6)	135.6(8)
Fe(2)−O(2)−Fe(8)	95.1(6)	Fe(6)−O(1)−Fe(8)	89.8(5)
Fe(2)−O(7)−Fe(3)	130.2(8)	Fe(6)−O(17)−Fe(7)	125.6(7)
Fe(2)−O(7)−Fe(4)	97.6(6)	Fe(6)−O(17)−Fe(8)	98.4(6)
Fe(3)−O(7)−Fe(4)	132.1(7)	Fe(7)−O(17)−Fe(8)	136.0(7)

has been seen only twice before in molecular chemistry;[41] its Fe−O−Fe angles (89.1(5)−90.7(7)°) deviate only slightly from the ideal 90°, and it lies very slightly (0.022 Å) above the Fe_4 plane. The $[Fe_3(\mu_3\text{-}O)]^{7+}$ triangular units are essentially isosceles (Table 2), the short separations being the

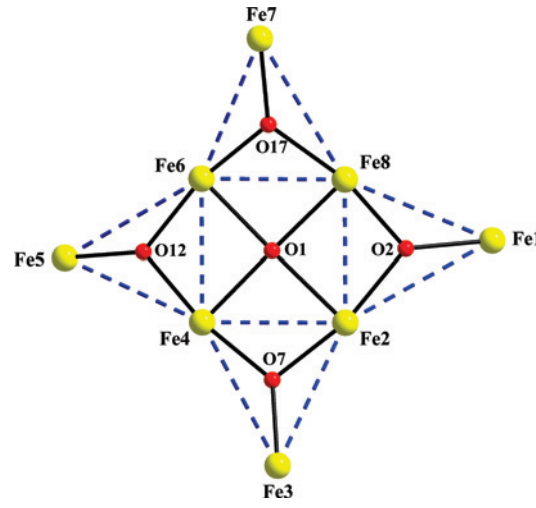

Figure 4. PovRay representation of the $[Fe_8O_5]^{14+}$ core of **3** emphasizing the "Christmas-star" topology, and highlighting the triangular $[Fe_3(\mu_3\text{-}O)]^{7+}$ and square-planar $[Fe_4(\mu_4\text{-}O)]^{10+}$ subcores (blue dashed lines).

Table 3. BVS for Fe[a] and Selected Oxygen[b] Atoms in **3**

atom	Fe^{II}	Fe^{III}
Fe1	2.67	2.96
Fe2	2.92	3.17
Fe3	2.59	2.88
Fe4	2.92	3.18
Fe5	2.65	2.95
Fe6	2.84	3.09
Fe7	2.60	2.89
Fe8	2.97	3.23

	BVS	assignment
O1	1.81	O^{2-}
O2	2.08	O^{2-}
O7	2.10	O^{2-}
O12	2.06	O^{2-}
O17	2.05	O^{2-}

[a] The underlined value is the one closest to the charge for which it was calculated. The oxidation state is the nearest whole number to the underlined value. [b] A BVS in the ~1.8−2.0, ~1.0−1.2, and ~0.2−0.4 ranges for an O atom is indicative of non-, single- and double-protonation, respectively, but can be altered somewhat by hydrogen bonding.

bis-oxide-bridged edges of the central square. This is also reflected in the geometry at the μ_3-O^{2-} ions, O2, O7, O12, and O17, which have Y-shaped geometry (largest Fe−O−Fe angles of 133.2(8), 132.2(8), 135.6(9), and 136.0(7)°, respectively) rather than the trigonal planar geometry usually seen in triangular metal carboxylates;[42] O2, O7, O12, and O17 are also slightly above their Fe_3 planes (0.002, 0.020, 0.024, and 0.019 Å, respectively). The Fe atoms are additionally bridged by eight η^1:η^1:μ $MeCO_2^-$ groups of two types: four bridge the four edges of the central Fe_4 square, and the remaining four bridge a central and external Fe atom. The peripheral ligation is completed by eight bidentate chelating en groups, two on each of the external Fe atoms. All Fe atoms are six-coordinate and near-octahedral. The Fe^{III} oxidation states and the degree of protonation of O^{2-} atoms were confirmed by Bond Valence Sum (BVS) calculations (Table 3).[43] Finally, there are several H-bonds involving en NH_2 groups and both $MeCO_2^-$ ligands and ClO_4^- anions; the former are intramolecular in nature, whereas in the latter they are intermolecular, serving to link neighboring Fe_8 cations in the crystal.

Complex **3** joins only a small family of cage-like Fe_8 clusters, most of which were reported only relatively recently, and these are listed in Table 4 for convenient comparison of their structural type; we have not included the Fe_8 molecular wheels in this list. Almost all complexes characterized magnetically have an $S = 0$ ground-state spin (*vide infra*). Complex **3** is an unusual structural type, as well as the largest homometallic cluster reported to date with en, and a similar core has been seen only in $[Fe_8O_5(O_2CMe)_8(tren)_4]^{6+}$ (tren is tris(2-aminoethyl)amine), reported briefly in 1994.[49]

The structure of the $[Fe_2O(O_2CBu^t)(en)_4]^{3+}$ cation of complex **4** is shown in Figure 5, and selected interatomic distances and angles are listed in Table 5. The cation consists of a $[Fe_2(\mu\text{-}O^{2-})(\mu\text{-}O_2CBu^t)]^{4+}$ core with octahedral geometry at each Fe^{III} atom completed by two chelating en groups. The $[Fe_2(\mu\text{-}O^{2-})(\mu\text{-}O_2CR)]^{3+}$ core is quite rare in Fe^{III} dinuclear chemistry, the common situation being a $[Fe_2(\mu\text{-}O^{2-})(\mu\text{-}O_2CR)_2]^{2+}$ core.[55] The Fe···Fe distance of 3.305(1) Å in **4** is typical for the $[Fe_2(\mu\text{-}O^{2-})(\mu\text{-}O_2CR)]^{3+}$ core: for example, it is 3.248(2), 3.343(1), and 3.243(1) Å in $[Fe_2OCl_2(O_2CPh)L(H_2O)_2]^+$ (L = bis-bpy),[56] $[Fe_2O(O_2CR)_4(dmpzH)_3]$ (dmpzH = 3,5-dimethylpyrazole),[57] and $[Fe_2O(O_2CMe)(tpa)_2]^{3+}$ ((tpa = tris(2-pyridylmethyl)-amine),[58] respectively. In contrast, the $[Fe_2(\mu\text{-}O^{2-})(\mu\text{-}O_2CR)_2]^{2+}$ core has appreciably smaller Fe···Fe separations, typically in the 3.063(2)−3.174(2) Å range.[55] There are several H-bonds involving en NH_2 groups in the cation of **4** and the NO_3^- counterions, and these serve to link neighboring Fe_2 cations in the crystal.

Magnetochemistry. dc Magnetic Susceptibility Studies. Variable-temperature dc magnetic susceptibility data were collected on powdered polycrystalline samples of **1a**−**4**, restrained in eicosane, in a 1 kG (0.1 T) field and in the 5.0−300 K range.

$\chi_M T$ for **1a**·2MeCN steadily decreases from 28.65 cm^3 K mol^{-1} at 300 K to 1.35 cm^3 K mol^{-1} at 5.0 K (Figure 6). The 300 K value is much less than the spin-only ($g = 2$) value of 43.75 cm^3 K mol^{-1} for 10 noninteracting Fe^{III} ions, indicating the strong antiferromagnetic interactions that are typical of mixed alkoxo/carboxylato-bridged Fe^{III} systems. The 5.0 K value is indicative of a singlet ($S = 0$) ground state, as expected for a ring containing an even number of Fe^{III} ions. This behavior is analogous to that of other Fe_{10} ferric wheels.[18−20,30a] For **3**·3MeCN, $\chi_M T$ rapidly decreases from 7.52 cm^3 K mol^{-1} at 300 K to 1.39 cm^3 K mol^{-1} at 5.0

(41) (a) Rambo, J. R.; Huffman, J. C.; Eisenstein, O.; Christou, G. *J. Am. Chem. Soc.* **1989**, *111*, 8027. (b) Cotton, F. A.; Feng, X. *Inorg. Chem.* **2001**, *29*, 3697. (c) Cotton, F. A.; Shang, M. *J. Am. Chem. Soc.* **1990**, *112*, 1584.

(42) (a) Cotton, F. A.; Wilkinson, G. *Advanced Inorganic Chemistry*; Wiley: New York, 1980; pp 154−155. (b) Cannon, R. D.; White, R. P. *Prog. Inorg. Chem.* **1988**, *36*, 195.

(43) (a) Brown, I. D.; Altermatt, D. *Acta Crystallogr.* **1985**, *B41*, 244. (b) Liu, W.; Thorp, H. H. *Inorg. Chem.* **1993**, *32*, 4102.

(44) Raptis, R. G.; Georgakaki, I. P.; Hockless, D. C. R. *Angew. Chem., Int. Ed.* **1999**, *38*, 1632.

(45) Gass, I. A.; Milios, C. J.; Whittaker, A. G.; Fabiani, F. P. A.; Parsons, S.; Murrie, M.; Perlepes, S. P.; Brechin, E. K. *Inorg. Chem.* **2006**, *45*, 5281.

(46) Brechin, E. K.; Knapp, M. J.; Huffman, J. C.; Hendrickson, D. N.; Christou, G. *Inorg. Chim. Acta* **2000**, *297*, 389.

(47) Ammala, P.; Cashion, J. D.; Kepert, C. M.; Moubaraki, M.; Murray, K. S.; Spiccia, L.; West, B. O. *Angew. Chem., Int. Ed.* **2000**, *39*, 1688.

(48) Hahn, F. E.; Jocher, C.; Lugger, T. *Z. Naturforsch. B.* **2004**, *59*, 855.

(49) Nair, V. S.; Hagen, K. S. *Inorg. Chem.* **1994**, *33*, 185.

(50) Schmitt, W.; Murugesu, M.; Goodwin, J. C.; Hill, J. P.; Mandel, A.; Bhalla, R.; Anson, C. E.; Heath, S. L.; Powell, A. K. *Polyhedron.* **2001**, *20*, 1687.

(51) Satcher, J. H., Jr.; Olmstead, M. M.; Droege, M. W.; Parkin, S. R.; Noll, B. C.; May, L.; Balch, A. L. *Inorg. Chem.* **1998**, *37*, 6751.

(52) Gautier-Luneau, I.; Fouquard, C.; Merle, C.; Pierre, J.- L.; Luneau, D. *Dalton Trans.* **2001**, 2127.

(53) (a) Murugesu, M.; Abbiud, K. A.; Christou, G. *Dalton Trans.* **2003**, 4552. (b) Ako, A. M.; Waldmann, O.; Mereacre, V.; Klöwer, F.; Hewitt, I. J.; Anson, C. E.; Güdel, H. U.; Powell, A. K. *Inorg. Chem.* **2007**, *46*, 756. (c) Jones, L. F.; Jensen, P.; Moubaraki, B.; Berry, K. J.; Boas, J. F.; Pilbrow, J. R.; Murray, K. S. *J. Mater. Chem.* **2006**, *16*, 2690.

(54) Taguchi, T.; Stamatatos, Th. C.; Abboud, K. A.; Jones, C. M.; Poole, K. M.; O'Brien, T. A.; Christou, G. *Inorg. Chem.* **2008**, *47*, 4095.

(55) Kurtz, D. M., Jr. *Chem. Rev.* **1990**, *90*, 585; and references therein.

(56) Seddon, E. J.; Yoo, J.; Folting, K.; Huffman, J. C.; Hendrickson, D. N.; Christou, G. *J. Chem. Soc., Dalton Trans.* **2000**, 3640; and references therein.

(57) Yoon, S.; Lippard, S. J. *J. Am. Chem. Soc.* **2004**, *126*, 2666.

(58) Sanders-Loehr, J.; Wheeler, W. D.; Shiemke, A. K.; Averill, B. A.; Loehr, T. M. *J. Am. Chem. Soc.* **1989**, *111*, 8084.

Table 4. Structural Types and Ground State S Values for Octanuclear Fe^{III} Clusters

complex[a,b]	core	type	S	ref
$[Fe_8O_4(pz)_{12}Cl_4]$	$[Fe_8(\mu_4\text{-}O)_4]^{16+}$	*c*	0	44
$[Fe_8O_4(sao)_8(py)_4]$	$[Fe_8(\mu_4\text{-}O)_4]^{16+}$	*c*	0	45
$[Fe_8O_4(O_2CPh)_{11}(hmp)_5]$	$[Fe_8(\mu_3\text{-}O)_4]^{16+}$	*d*	0	46
$[Fe_8O_4(O_2CMe)_{12}(hmp)_4]$	$[Fe_8(\mu_3\text{-}O)_4]^{16+}$	*d*	0	46
$[Fe_8O_4(O_2CPh)_{14}(OR)_2(ROH)_2]$	$[Fe_8(\mu_4\text{-}O)_2(\mu_3\text{-}O)_2]^{16+}$	*e*	0	47
$[Fe_8O_4(L)_4Cl_8]$	$[Fe_8(\mu_4\text{-}O)_4]^{16+}$	*c*	n.r.	48
$[Fe_8O_5(O_2CMe)_8(tren)_4]^{6+}$	$[Fe_8(\mu_4\text{-}O)(\mu_3\text{-}O)_4]^{14+}$	*f*	n.r.	49
$[Fe_8O_4(OH)_4(Me_2hda)_4(en)_4]$	$[Fe_8(\mu_3\text{-}O)_4(\mu\text{-}OH)_4]^{12+}$	*g*	0	50
$[Fe_8O_4(OH)_4(O_2CMe)_4(BMDP)_4]^{4+}$	$[Fe_8(\mu\text{-}O)_4(\mu\text{-}OH)_4]^{12+}$	*h*	n.r.	51
$[Fe_8O_2(OH)_{12}(tacn)_6]^{8+}$	$[Fe_8(\mu_3\text{-}O)_2(\mu\text{-}OH)_{12}]^{8+}$	*i*	10	12a
$[Fe_8O_2(OH)_2(O_2CMe)_2(cit)_6(im)_2]^{8-}$	$[Fe_8(\mu_3\text{-}O)_2(\mu\text{-}OH)_2]^{18+}$	*j*	0	52
$[Fe_8O_3(O_2CPh)_9(tea)(teaH)_3]$	$[Fe_8(\mu_4\text{-}O)_3]^{18+}$	*k*	0	53a
$[Fe_8O_3(O_2CCMe_3)_6(N_3)_3(tea)(teaH)_3]$	$[Fe_8(\mu_4\text{-}O)_3]^{18+}$	*k*	n.r.	53b
$[Fe_8O_3(O_2CEt)_6F_3(tea)(teaH)_3]$	$[Fe_8(\mu_4\text{-}O)_3]^{18+}$	*k*	0	53c
$[Fe_8O_3(OMe)(pdm)_4(pdmH)_4(MeOH)_2]^{5+}$	$[Fe_8(\mu_4\text{-}O)(\mu_3\text{-}O)_2]^{18+}$	*l*	0	54
$[Fe_8O_5(O_2CMe)_8(en)_8]^{6+}$	$[Fe_8(\mu_4\text{-}O)(\mu_3\text{-}O)_4]^{14+}$	*f*	0	t.w.

[a] Counterions omitted. [b] Abbreviations: n.r. = not reported; t.w. = this work; pzH = pyrazole; $saoH_2$ = salicylaldehyde oxime; py = pyridine; LH_2 = (2-aminoethyl)-2-hydroxyethyl-(3-hydroxypropyl)amine; tren = tris(2-aminoethyl)amine; Me_2hdaH_3 = *N*-(5-allyl-2-hydroxy-3-methoxybenzyl)iminodiacetic acid; en = ethylenediamine; BMDPH = *N*,*N*,*N*′-tris((*N*-methyl)-2-benzimidazolylmethyl)-*N*′-methyl-1,3-diamino-2-propanol; tacn = 1,4,7-triazacyclononane; $citH_4$ = citric acid; im = imidazole; $teaH_3$ = triethanolamine; $pdmH_2$ = 2,6-pyridinedimethanol. [c] $[Fe_4(\mu_3\text{-}O)_4]^{4+}$ cube within an Fe_4 tetrahedron. [d] Four linked $[Fe_3(\mu_3\text{-}O)]^{7+}$ triangles. [e] Double-butterfly. [f] Four vertex-fused $[Fe_3(\mu_3\text{-}O)]^{7+}$ triangles about a $\mu_4\text{-}O^{2-}$ ion. [g] Distorted Fe_8 cubane. [h] Distorted Fe_8 square. [i] Four Fe about an Fe_4 butterfly. [j] Two linked Fe_4 tetrahedra. [k] Three edge-sharing Fe_4 tetrahedra. [l] $[Fe_4(\mu_4\text{-}O)]$ tetrahedron fused with two $[Fe_3(\mu_3\text{-}O)]^{7+}$ triangles.

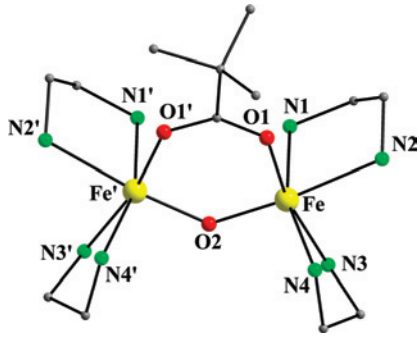

Figure 5. Labeled PovRay representation of complex **4**, with H atoms omitted for clarity.

Table 5. Selected Interatomic Distances (Å) and Angles (deg) for **4**

parameter[a]		parameter	
Fe···Fe′	3.305(1)	Fe−N(2)	2.249(2)
Fe−O(1)	2.046(1)	Fe−N(3)	2.173(2)
Fe−O(2)	1.800(8)	Fe−N(4)	2.151(2)
Fe−N(1)	2.153(2)		
Fe−O(2)−Fe′	133.3(1)	O(2)−Fe−N(2)	174.1(8)
O(1)−Fe−N(3)	167.1(6)	N(1)−Fe−N(4)	161.4(7)

[a] Primed and unprimed atoms are related by the inversion center.

K (Figure 7). Again, the 300 K value is much less than the spin-only value of 35.00 cm^3 K mol^{-1} for eight noninteracting Fe^{III} ions, indicating strong antiferromagnetic exchange interactions and a singlet ground state. For complex **4**, $\chi_M T$ decreases rapidly from 0.93 cm^3 K mol^{-1} at 300 K to 0.08 cm^3 K mol^{-1} at 5.0 K (Figure 8). The 300 K value is once more much less than the spin-only value of 8.75 cm^3 K mol^{-1} for two noninteracting Fe^{III} ions, again indicating strong antiferromagnetic interactions and an $S = 0$ ground state.

The isotropic (Heisenberg) spin Hamiltonian for dinuclear complex **4** is given by eq 8,

$$H = -2J\hat{S}_1 \cdot \hat{S}_2 \quad (8)$$

$$E(S_T) = -JS_T(S_T + 1) \quad (9)$$

where J is the exchange interaction parameter and $S_1 = S_2 = 5/2$. This gives total spin (S_T) states of $S_T = 5, 4, 3, 2, 1, 0$, with relative energies $E(S_T)$ given by eq 9. A theoretical χ_M versus T expression appropriate for a d^5-d^5 dimer has been previously derived from the use of eq 9 and the Van

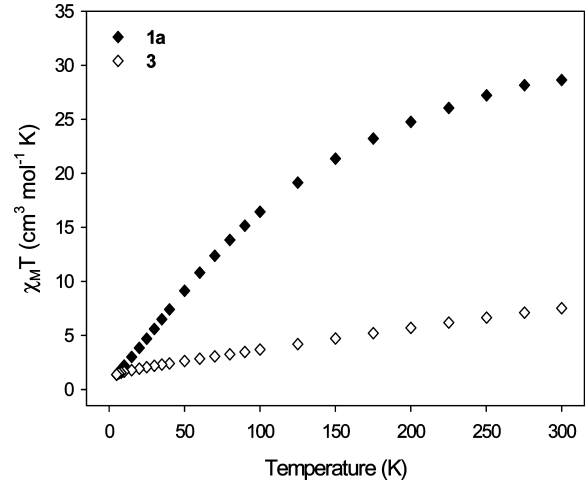

Figure 6. Plots of $\chi_M T$ vs T for complexes **1a** (◆) and **3** (◇).

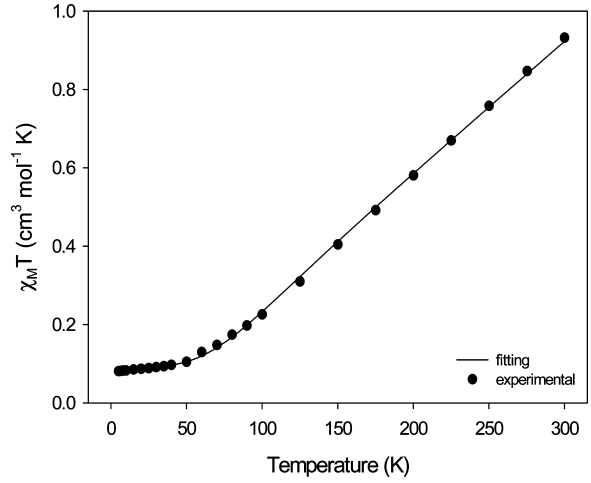

Figure 7. Plot of $\chi_M T$ vs T for complex **4**. The solid line is the fit of the data; see the text for the fit parameters.

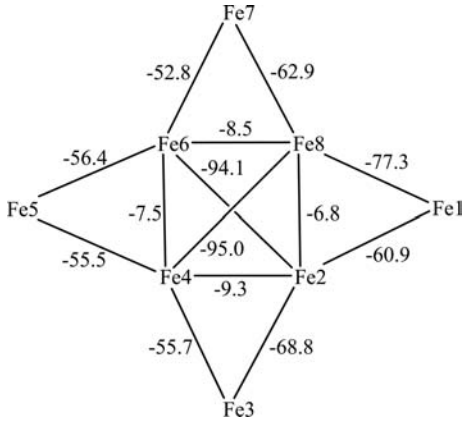

Figure 8. Summary of *J* exchange constants obtained for complex **3** from the ZILSH calculations.

Vleck equation,[56] and this was modified to include a fraction (p) of paramagnetic impurity (assumed to be a mononuclear Fe^{III}) and temperature-independent paramagnetism (TIP); the latter was kept constant at 500×10^{-6} cm^3 K mol^{-1}. The resulting equation was used to fit the experimental χ_M versus T data for **4**. The obtained fit (solid line in Figure 7) gave $J = -107.7(5)$ cm^{-1}, $g = 2.05(4)$, and $p = 0.011(3)$. The complex is thus confirmed to be very strongly antiferromagnetically coupled with an $S_T = 0$ ground state and an $S = 1$ first excited state at 215.4 cm^{-1} higher energy.

The experimental J value for complex **4** is as expected from empirical magnetostructural correlations.[59] Using the J versus P relationship reported by Gorun and Lippard (eq 10),[59a]

$$-J = A \exp(BP) \qquad (10)$$

where P is defined as half the shortest superexchange pathway between the two Fe^{III} ions, $A = 8.763 \times 10^{11}$, $B = -12.663$, and J is based on the spin Hamiltonian of eq 8. For **4**, half the Fe−O2−Fe′ pathway distance is 1.800(8) Å, giving a predicted $J = -110.5(5)$ cm^{-1}, very close to the experimental $J = -107.7(5)$ cm^{-1}. The latter is similar to the values obtained for other compounds with the $[Fe_2(\mu\text{-}O)(\mu\text{-}O_2CR)]^{3+}$ core.[55]

Theoretical Studies. The $S = 0$ ground states of complexes **1**, **2**, and **4** are as they should be for antiferromagnetically coupled Fe^{III}_x (x = even) wheels and dinuclear complexes where antiparallel spin alignment of neighboring spins is to be expected. However, the spin alignments within **3** giving its observed $S = 0$ ground state are not so intuitively obvious given the extensive spin frustration expected in an antiferromagnetically coupled cluster consisting of so many fused Fe_3 triangular units; note that the central Fe_4 square can also be described as fused triangular units. Therefore, to probe the exact nature of the $S = 0$ ground state of **3**, we have carried out theoretical calculations using the semiempirical ZILSH method.[26] A ZILSH calculation on the ferric wheel $[Fe_{10}(OMe)_{20}(O_2CBu^t)_{10}]$ has already been published.[30a]

Calculations were performed on 29 spin components of **3** so that estimates of all parameters in eq 1 could be obtained (E_0 and 28 pairwise exchange constants). The spin components used were the one with all unpaired spins aligned parallel ("high spin", HS) and all components with unpaired spin on two Fe^{III} atoms reversed (antiparallel) relative to the others (e.g., unpaired spin on Fe1 and Fe2 reversed, those on Fe1 and Fe3 reversed, etc.). Calculated energies and local spin densities are given in Table 6. A summary of these results is as follows: the HS component is substantially higher in energy than the other components, indicating that the exchange interactions in **3** are predominantly antiferromagnetic. The spin densities have magnitudes close to the formal value of five expected for high spin (d^5) Fe^{3+} ions but are reduced below this number by spin delocalization, as found with ZILSH for other complexes of Fe^{3+} ions.[22,26,30,54] The signs of the local spin densities indicate the relative directions of the spin moments of the iron ions and show that the correct spin distributions were obtained for all the spin components.

Nonzero exchange constants obtained from the data of Table 6 are presented in Table 7 and Figure 8, using the numbering scheme of Figure 4. Focusing first on interactions within the four outer triangular subunits of the Fe_8 core (Fe1, Fe2, Fe8/Fe2, Fe3, Fe4/Fe4, Fe5, Fe6, and Fe6, Fe7, Fe8), they approximately follow the virtual S_4 symmetry of the complex and so are similar for the four triangular units; further discussion is thus limited to the Fe1−Fe2−Fe8 unit. The J_{28} pathway is bridged by both μ_3-O^{2-} and μ_4-O^{2-} ions, while the J_{12} and J_{18} pathways are bridged by only one μ_3-O^{2-} ion; there is also a triatomic-bridging $MeCO_2^-$ group bridging the Fe2Fe8 and Fe1Fe8 pairs. Consideration of the relative magnitudes of the exchange constants shows a large difference between the J_{28} (−6.8 cm^{-1}) and the J_{12}/J_{18} interactions (−60.0 and −77.3 cm^{-1}, respectively), which is consistent with established magnetostructural correlations between stronger J values and both shorter Fe−O bond distances and larger Fe−O−Fe angles in the oxide-mediated pathways[26,59−61] ($J_{18} = -77.3$ cm^{-1}, average Fe−O = 1.853 Å, average Fe−O−Fe = 131.7°; $J_{12} = -60.9$ cm^{-1}, average Fe−O = 1.922 Å, average Fe−O−Fe = 133.2°; $J_{28} = -6.8$ cm^{-1}, average Fe−O = 1.997 Å, average Fe−O−Fe = 92.7°). Thus, the J_{28} interaction is particularly weak because the Fe−O−Fe angles in this pathway are extremely small, only slightly larger than 90°, and the average Fe−O distance of ∼2.0 Å is very long. This value of J_{28} in **3** is similar to those found for antiferromagnetic oxide-mediated "body-body" (J_{bb}) interactions in Fe_4 butterfly complexes, which have similarly long Fe−O distances and small Fe−O−Fe angles (e.g., $[Fe_4O_2(O_2CMe)_7(bpy)_2]^+$, $J_{bb} = -8.9$ cm^{-1}, 1.937 Å, 95.0°;[62] $[Fe_4O_2(O_2CPh)_7(phen)_2]^+$, $J_{bb} = -2.4$ cm^{-1}, 1.934 Å, 96.3°.[63]

The central Fe_4 subunit consists of Fe2, Fe4, Fe6, and Fe8 and is roughly a square. As discussed above, the exchange

(59) (a) Gorun, S. M.; Lippard, S. J. *Inorg. Chem.* **1991**, *30*, 1625. (b) Weihe, H.; Güdel, H. U. *J. Am. Chem. Soc.* **1998**, *120*, 2870.

(60) Weihe, H.; Güdel, H. U. *J. Am. Chem. Soc.* **1997**, *119*, 6539.

(61) Werner, R.; Ostrovsky, S.; Griesar, K.; Haase, W. *Inorg. Chim. Acta* **2001**, *326*, 78.

(62) McCusker, J. K.; Vincent, J. B.; Schmitt, E. A.; Mino, M. L.; Shin, K.; Coggin, D. K.; Hagen, P. M.; Huffman, J. C.; Christou, G.; Hendrickson, D. N. *J. Am. Chem. Soc.* **1991**, *113*, 3012.

(63) Boudalis, A. K.; Lalioti, N.; Spyroulias, G. A.; Raptopoulou, C. P.; Terzis, A.; Bousseksou, A.; Tangoulis, V.; Tuchagues, J.-P.; Perlepes, S. P. *Inorg. Chem.* **2002**, *41*, 6474.

Table 6. Results of ZILSH Calculations on Complex **3**

component[a]	energy (cm^{-1})[b]	M_1[c]	M_2	M_3	M_4	M_5	M_6	M_7	M_8
HS	9083.6[d]	4.29	4.43	4.32	4.42	4.29	4.45	4.32	4.42
1,2	3989.8	−4.24	−4.32	4.27	4.42	4.29	4.37	4.32	4.38
1,3	3948.8	−4.22	4.37	−4.24	4.40	4.29	4.44	4.31	4.38
1,4	2122.9	−4.22	4.40	4.29	−4.29	4.26	4.44	4.31	4.31
1,5	4131.3	−4.22	4.39	4.31	4.40	−4.23	4.42	4.31	4.38
1,6	2180.7	−4.22	4.32	4.31	4.42	4.26	−4.31	4.28	4.38
1,7	4116.9	−4.22	4.39	4.31	4.42	4.29	4.42	−4.25	4.35
1,8	4416.6	−4.26	4.39	4.31	4.34	4.29	4.44	4.28	−4.31
2,3	4564.8	4.26	−4.32	−4.28	4.39	4.29	4.37	4.32	4.42
2,4	583.0	4.26	−4.29	4.25	−4.29	4.26	4.37	4.31	4.35
2,5	2324.9	4.26	−4.29	4.27	4.39	−4.23	4.34	4.32	4.42
2,6	3832.4	4.26	−4.36	4.27	4.42	4.26	−4.38	4.28	4.42
2,7	2215.3	4.26	−4.29	4.27	4.42	4.29	4.34	−4.25	4.39
2,8	0.0	4.22	−4.29	4.27	4.35	4.29	4.37	4.28	−4.27
3,4	4396.1	4.29	4.39	−4.26	−4.31	4.26	4.44	4.32	4.34
3,5	4452.3	4.29	4.39	−4.24	4.37	−4.23	4.42	4.32	4.42
3,6	2420.4	4.29	4.32	−4.24	4.40	4.26	−4.31	4.28	4.41
3,7	4300.8	4.29	4.39	−4.24	4.40	4.29	4.42	−4.25	4.39
3,8	1889.2	4.24	4.39	−4.24	4.32	4.29	4.44	4.28	−4.27
4,5	4636.7	4.29	4.43	4.29	−4.31	−4.26	4.41	4.32	4.34
4,6	885.7	4.29	4.36	4.29	−4.29	4.23	−4.31	4.28	4.35
4,7	2548.5	4.29	4.43	4.29	−4.29	4.26	4.42	−4.25	4.31
4,8	3614.8	4.24	4.43	4.29	−4.36	4.25	4.44	4.28	−4.35
5,6	4729.8	4.29	4.35	4.31	4.40	−4.25	−4.33	4.28	4.41
5,7	4607.7	4.29	4.42	4.31	4.40	−4.23	4.39	−4.25	4.39
5,8	2124.9	4.24	4.42	4.31	4.32	−4.23	4.41	4.28	−4.27
6,7	4516.1	4.29	4.35	4.31	4.42	4.26	−4.33	−4.28	4.38
6,8	429.6	4.24	4.35	4.31	4.35	4.26	−4.31	4.25	−4.28
7,8	4330.5	4.24	4.42	4.32	4.34	4.29	4.42	−4.28	−4.30

[a] HS indicates the spin component with all spins aligned parallel. Numbers indicate the two metal atoms whose unpaired spins are reversed relative to the other unpaired spins. See Figure 4 for the numbering scheme. [b] Relative energy (cm^{-1}). [c] z component of spin for Fe1 from ZILSH calculations. [d] Absolute energy of HS component (a.u.) is −931.00424614.

Table 7. Nonzero Exchange Constants Calculated for Complex **3** with ZILSH, and Associated Spin Couplings $\langle \hat{S}_A \cdot \hat{S}_B \rangle$ Computed for the Ground State Spin Wavefunction

interaction[a]	J (cm^{-1})	$\langle \hat{S}_A \cdot \hat{S}_B \rangle$[b]
J_{12}	−60.9	−5.11
J_{18}	−77.3	−5.81
J_{28}	−6.8	0.72
J_{23}	−68.8	−5.18
J_{24}	−9.3	−0.31
J_{34}	−55.7	−4.92
J_{45}	−55.5	−5.57
J_{46}	−7.5	0.12
J_{56}	−56.4	−4.89
J_{67}	−52.8	−5.09
J_{68}	−8.5	−0.31
J_{78}	−62.9	−4.95
J_{26}	−94.1	−7.18
J_{48}	−95.0	−7.09

[a] $-2J$ convention; see Figure 4 for the numbering scheme. [b] Spin couplings were computed from the ground $S = 0$ spin eigenstate obtained from diagonalization of the Heisenberg Hamiltonian.

pathways along the edges of the square are mediated by the central μ_4-O^{2-} ion and the μ_3-O^{2-} ion of the adjacent triangular unit, as well as a $MeCO_2^-$ group; these are the weakest J_{24}, J_{28}, J_{46}, and J_{68} interactions of Table 7. If we now consider the diagonal interactions across the square J_{26} and J_{48}, we see that these Fe2/Fe6 and Fe4/Fe8 pairs are bridged by the central μ_4-O^{2-} ion with essentially linear Fe−O−Fe angles. These large angles lead to J_{26} and J_{48} being the strongest exchange interactions in **3** (~ -95 cm^{-1}). Linear or nearly linear Fe−O−Fe angles (>170°) are found in several μ-O^{2-} bridged Fe^{III}_2 complexes,[64] and these have exchange constants of similar magnitude to J_{26} and J_{48} ($\sim$100 cm^{-1}).

The spin alignments giving rise to the $S = 0$ ground state of **3** are not obvious owing to the large number of antiferromagnetic exchange constants of similar magnitude in the complex and the resulting spin frustration effects expected within its many triangular units. In fact, it is not obvious even what the ground state would be merely by considering the J values of Table 7. Spin eigenstate calculations were therefore carried out to determine the ground-state spin and gain a more detailed picture of spin alignments in the complex.

The J values of Table 7 were substituted into the Heisenberg Hamiltonian, and spin eigenstates were obtained for the lowest energy state of each spin with the Davidson algorithm. The ground state was found by these calculations to have $S = 0$, in agreement with the experimental magnetic studies (vide supra), with the $S = 1$ first excited state being 19.2 cm^{-1} higher in energy. The ground state $S = 0$ wave function is very complicated. The leading components have coefficients with magnitudes on the order of 0.045, representing contributions of 0.002% to the wave function. There are 748 components making contributions within 1 order of magnitude of this, and 68 components making contributions of between 0.001 and 0.002%. As is typical for singlet states, the wave function consists of pairs of components with equal contributions in which the z components of the spin at each

(64) (a) Strauss, S. H.; Pawlik, M. J.; Skowyra, J.; Kennedy, J. R.; Anderson, O. P.; Spartalian, K.; Dye, J. L. *Inorg. Chem.* **1987**, *26*, 724. (b) Ou, C. C.; Wollmann, R. G.; Hendrickson, D. N.; Potenza, J. A.; Schugar, H. J. *J. Am. Chem. Soc.* **1978**, *100*, 4717. (c) Mukherjee, R. N.; Stack, T. D. P.; Holm, R. H. *J. Am. Chem. Soc.* **1988**, *110*, 1850. (d) Hazell, A.; Jensen, K. B.; McKenzie, C. J.; Toftlund, H. *Inorg. Chem.* **1994**, *33*, 3127.

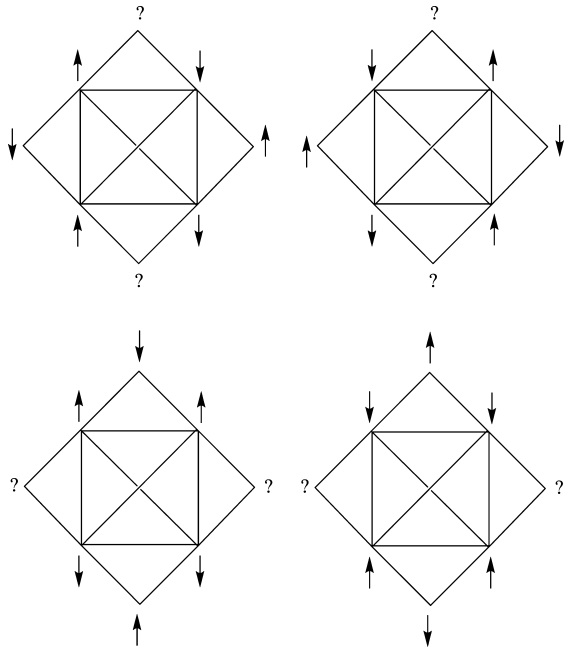

Figure 9. Components making significant contributions to the $S = 0$ ground state of **3**. See the text for discussion.

spin carrier are reversed relative to each other; for example, $\psi_{S=0} = 2^{-1/2}(|\alpha\beta\rangle - |\beta\alpha\rangle)$ for two singlet-coupled electrons. This leads to average z components of spin of zero for each Fe^{3+} ion, which makes it difficult to analyze the ground-state spin alignments from the wave function itself. In the past, we have used the expectation values of the spin couplings between metal ions, $\langle \hat{S}_A \cdot \hat{S}_B \rangle$, computed for the wave function, to analyze spin alignments in $S = 0$ ground states.[30,31] The spin coupling also provides a convenient probe for spin frustration because it represents the actual alignment of two spins, whereas the exchange constant J_{AB} indicates their preferred alignment. Thus, pathways with J and $\langle \hat{S}_A \cdot \hat{S}_B \rangle$ of different sign are frustrated.

Spin couplings $\langle \hat{S}_A \cdot \hat{S}_B \rangle$ computed for the ground $S = 0$ state are also given in Table 7. It is useful in analyzing these results to compare to the spin couplings expected for a pair of perfectly parallel and antiparallel Fe^{3+}spins of +6.25 and −8.75, respectively. We have previously observed, for example, that $\langle \hat{S}_A \cdot \hat{S}_B \rangle = +6.25$ for an antiferromagnetically coupled Fe^{III}_2 pair indicates a completely frustrated exchange pathway.[31] The strongest interactions in **3** are J_{26} and J_{48}, across the diagonals of the central Fe_4 square (vide supra). The spin couplings for these pathways approach the value of −8.75 expected for two singlet-coupled Fe^{3+} ions, showing a strong tendency for these diagonally opposite Fe^{3+} spins to align antiparallel. Interestingly, spin couplings for pathways along each side of this unit (Fe2−Fe4, Fe4−Fe6, Fe6−Fe8, Fe2−Fe8) are very close to zero, indicating little preference for spins at adjacent corners of the square to align either parallel or antiparallel. Components similar to those illustrated pictorially in Figure 9 can thus be expected to make among the larger contributions to the wave function, though it is difficult to a priori estimate the exact z components of spin of each metal ion, given the large number of strong and competing antiferromagnetic interactions.

Considering next the spins on atoms at the apexes of each triangular subunit, two of these in each case will clearly align as indicated with up or down arrows in Figure 9, top and bottom, given the strong antiferromagnetic interactions between these ions and those in the central unit with parallel spins. The other two, however, are acted on by similarly strong antiferromagnetic interactions with ions in the central unit with antiparallel spins and so will be in some intermediate orientation (indicated with question marks). As the wave function will contain similar contributions from all four components shown in Figure 9, the spin of each apical ion will be in some intermediate orientation between $m_A = +5/2$ and $m_A = -5/2$. Considering again the atoms in the central Fe_4 unit, the interactions between these and the apical atoms are strong enough that they in turn cause the spins of ions in the central unit to be in intermediate orientations as well. This is indicated by the values of $\langle \hat{S}_A \cdot \hat{S}_B \rangle$ for apical and central unit ions, which, while negative, are substantially reduced from the value of −8.75 expected for perfect antiparallel alignment of two spins with $S_A = S_B = 5/2$. It is also clear that the exchange interactions acting on the four ions in the central unit are closely balanced because the interactions between adjacent ions in this unit have no preference to align either parallel or antiparallel, as shown by spin couplings that are approximately zero.

The picture of spin interactions in **3** constructed on the basis of Figure 9 is strongly supported by a more detailed analysis of the ground-state wave function. Sixty eight components make contributions of similar size to those of the leading component, as mentioned above, and local z components of spin of all possible values occur within each of these components. Considering only those components with m_1 positive, so that components with exactly reversed spin alignments making equal contributions to the wave function (as in $\psi_{S=0} = 2^{-1/2}(|\alpha\beta\rangle - |\beta\alpha\rangle)$ for two singlet-coupled electrons) are not considered, m_2 ranges from −5/2 to 5/2 within this set of components, as do m_3−m_8. The same is true if only components with positive values of m_2 are considered, and so on. It is important to note that all of these components make roughly equal contributions to the ground-state wave function. Finally, components with all local z components of spin with magnitude of 5/2 make very small contributions to the wave function, at most 2 orders of magnitude smaller than the contributions of the 68 leading components.

There is a sharp contrast between the wave function just described and the wave function for the $S = 0$ ground state of $[Fe_6O_2(OH)(O_2CPh)_9(hep)_4]$ (hepH = 2-(2-hydroxyethyl)-pyridine).[30b] As thoroughly detailed in this previous paper, this Fe_6 complex has two antiferromagnetic pathways that are completely frustrated (i.e., the spins aligned perfectly parallel), while all other pathways have spins aligned perfectly antiparallel. This is reflected in the spin couplings found for that complex, which were +6.21 for the frustrated pathways and on the order of −7.00 for all other strongly interacting pathways (see Table 6 of ref 30b). By far the largest contributions to the ground-state wave function of this complex have all local z components of spin with

magnitude 5/2. The ground state has $S = 0$ because of the relative locations of the strongly frustrated pathways; a different arrangement of these pathways in closely related compounds leads to a ground state with $S = 5$.[30b]

It appears that none of the pathways in **3** are strongly frustrated in the sense that their spins are aligned exactly parallel despite antiferromagnetic exchange constants. This would lead to large, positive $\langle \hat{S}_A \cdot \hat{S}_B \rangle$ values approaching the value of +6.25 expected for parallel alignment in a system of two spins with $S_A = S_B = 5/2$, as seen for the strongly frustrated pathways in $[Fe_6O_2(OH)(O_2CPh)_9(hep)_4]$. No such spin couplings were found for any of the pathways in **3**. Only the spins of ions on opposite corners of the square central subunit of the core are strongly disposed to align antiparallel ($\langle \hat{S}_A \cdot \hat{S}_B \rangle \approx -7.00$). All other pairs of spins are either weakly disposed to align antiparallel ($\langle \hat{S}_A \cdot \hat{S}_B \rangle \approx -5.00$), or in the case of the pathways along the edges of the central unit, have very little preference for either parallel or antiparallel alignment ($\langle \hat{S}_A \cdot \hat{S}_B \rangle \approx 0$). The spin alignments in the $S = 0$ ground state in **3** thus arise from the exchange interactions more or less canceling each other out, rather than the arrangement of pathways that are strongly frustrated or strongly disposed toward antiparallel spin alignment, as in $[Fe_6O_2(OH)(O_2CPh)_9(hep)_4]$ and related compounds.

Conclusions

A convenient and high yield (>85%) procedure has been developed to the Fe_{10} family of single-strand "ferric wheels" involving the methanolysis under basic conditions of $[Fe_3O(O_2CR)_6(H_2O)_3]^+$ salts in MeOH. The two benefits of this approach, in addition to the high yields, are that (i) the $[Fe_3O(O_2CR)_6(H_2O)_3]^+$ salts are themselves accessible in high (typically >90%) yield with a variety of R groups starting from simple Fe^{III} salts and sodium carboxylates; and that (ii) the Fe_{10} products are insoluble in MeOH and thus precipitate from the reaction medium, allowing ready separation from excess reagents and byproducts of the synthesis. As a result, the purity of even the crude materials is high. The combination of points (i) and (ii) thus makes available for the first time large quantities of Fe_{10} ferric wheels with a variety of R groups. In addition, we have established that carboxylate substitution can be carried out on the acetate derivative, providing a convenient route to isotopically labeled (e.g., deuterated) and related derivatives without the need and expense of going via the corresponding $[Fe_3O(O_2CR)_6(H_2O)_3]^+$ salt.

The availability of large quantities of pure materials has also made a convenient option the use of Fe_{10} "ferric wheels" as starting materials to new products, and we have reported two preliminary investigations as "proof-of-feasibility", the reactions with phenol and en. These have given a variety of new Fe_x clusters. As an added convenience, we have shown for most of these reactions that the Fe_{10} "ferric wheel" need not be previously isolated but may be generated *in situ* before further reaction. There are many additional and potentially interesting reactions of Fe_{10} wheels that have been envisaged, and we anticipate that this will prove to be a rich source of a variety of interesting new Fe_x clusters and related products in the future as this chemistry is investigated systematically.

The magnetic studies of complexes **1a**−**4** have revealed that all of them have an $S = 0$ ground state, as expected for oxide/alkoxide bridged Fe^{III} systems with an even number of metal atoms. However, as part of our interest in not just what the ground state of a particular cluster topology is but how exactly it comes about,[30,54,65] we have analyzed the Fe_8 product **3** with the "Christmas star" topology using the ZILSH method. The latter is particularly useful for higher nuclearity systems, and we have rationalized the observed $S = 0$ ground state in terms of the computed exchange parameters and the resulting spin frustration occurring within the core. In contrast to many other Fe_x complexes we have studied in recent years, the situation in **3** is a particularly complex one, as reflected in the very large number of components contributing to the ground-state wave function. As such, it is a nevertheless informative demonstration of the extreme complexity possible in some spin frustrated metal clusters. Other studies with Fe_x wheels and their derivatives and products are currently in progress and will be reported in due course.

Acknowledgment. This work was supported by NSF (CHE-0414555 to G.C.) and an IBM Shared University Research grant to IU (T.O'B.). K.M.P. acknowledges funding from the Undergraduate Research Opportunities Program at IUPUI.

Supporting Information Available: X-ray crystallographic files in CIF format for complexes **1**·10MeCN, **2**·H_2O·CH_2Cl_2, **3**·8MeCN, and **4**. This material is available free of charge via the Internet at http://pubs.acs.org.

IC801038R

(65) (a) Stamatatos, Th. C.; Poole, K. M.; Foguet-Albiol, D.; Abboud, K. A.; O'Brien, T. A.; Christou, G. *Inorg. Chem.* **2008**, *47*, 6593. (b) Stamatatos, Th. C.; Poole, K. M.; Abboud, K. A.; Wernsdorfer, W.; O'Brien, T. A.; Christou, G. *Inorg. Chem.* **2008**, *47*, 5006. (c) Foguet-Albiol, D.; O'Brien, T. A.; Wernsdorfer, W.; Moulton, B.; Zaworotko, M. J.; Abboud, K. A.; Christou, G. *Angew. Chem., Int. Ed.* **2005**, *44*, 897. (d) Bagai, R.; Daniels, M. R.; Abboud, K. A.; Christou, G. *Inorg. Chem.* **2008**, *47*, 3318; and references therein.